Copyright

by

Artur Widera

2001

Design and Construction of a Modular Spin – Flip Zeeman Slower

by

Artur Widera,

Thesis

Presented to the Faculty of the Graduate School of

The University of Texas at Austin

in Partial Fulfillment

of the Requirements

for the Degree of

Master of Arts

The University of Texas at Austin

August 2001

Design and Construction of a Modular Spin – Flip Zeeman Slower

Approved by
Supervising Committee:

_____

_____

Für meine Eltern

Acknowledgments

First of all, I want to thank my supervisor, Mark Raizen. I received a lot of support from him, and basically everything I know about experimental physics, I have learned in his lab; I especially appreciate his attitude that besides the research, teaching in the lab is of great importance. Moreover, in his lab there is a very pleasant atmosphere possible that I enjoyed very much.
I had some big private problems during that year, and his immediate and uncomplicated help enabled me to stay in Austin and to finish my work in his lab.

The great atmosphere was also due to the people that worked with me. I want to say thanks to Kevin and Artem, with whom I worked closely together and who helped me winding coils, preparing the circuit boards, and wherever else I needed help.
A big thanks goes to Braulio, who spent many hours helping me to make my circuit boards work. Without him I would probably still unavailingly try to find the bugs. I learned a whole lot from him.
Many thanks to Windell, Dan, and Jay for answering all my questions and for the many suggestions to make my project work.
All the other people who worked in the lab were always helpful and a pleasure to talk to – whether it was about physics or the rest of the world. Thanks to Martin, Valery, Patrik, Todd, Chuanwei, Greg, Adrienne, and Julie.

Everything I know about designing and machining, I learned from Jack in the students' shop. I always looked forward to working there, even if things didn't work for the third or fourth time. Jack is the perfect person for this job, and I will miss him and the shop.

Ein großes Dankeschön geht an meine Familie. Wir hatten eine sehr schwere Zeit durchzustehen als mein Vater während des Jahres hier starb. Ohne eure Hilfe hätte ich meine Arbeit hier nicht abschließen können oder wollen.

Thanks to everybody who helped reading my thesis and correcting the $\lim_{n\to\infty} n$ mistakes in it, and to Prof. Frommhold who spontaneously agreed to read my thesis.
I want to thank Prof. Böhm and Prof. Langhoff from the Universität Würzburg for their work that made this exchange possible.
I acknowledge the Studienstiftung des deutschen Volkes (German National Merit Foundation) for their financial support.

Artur Widera

The University of Texas at Austin
August 2001

Design and Construction of a Modular Spin – Flip Zeeman Slower

Artur Widera, M.A.
The University of Texas at Austin, 2001

Supervisor: Prof. Mark Raizen

This thesis describes the design and construction of a Zeeman slower for sodium atoms. The slower is based on a modular design of thirteen coils driven by different currents; the feasability to change those currents allows for high flexibility during operation. Compared with other working Zeeman slowers for sodium, the one presented here has a rather low power dissipation of less than 500 W and a high range of slowable velocities up to 1000 $\frac{\mathrm{m}}{\mathrm{s}}$. Moreover, the modular design allows for quick repairs in case of a failure of the slower.

After a brief introduction to the theory of laser cooling, the main considerations that gave rise to the design of the slower will be presented, as will simulations used in the design process. The main parameters that led to the design as it works today – consisting of magnetic coils and an electronical regulation – will be discussed. Finally, experimental data from field measurements on the slower will be presented.

Contents

Acknowledgments **vi**

Abstract **viii**

Chapter 1 Introduction **1**

1.1 The Concept of Laser Cooling 1

1.2 Doppler Shift 2

1.3 Atoms in a Magnetic Field 5

1.4 Real Systems 8

1.4.1 Slowing Transition 8

1.4.2 Repumping 9

1.4.3 Transverse Heating 10

1.5 Limitations 11

1.5.1 Number of Atoms versus Background Pressure 11

1.5.2 Cooling Limit 12

1.5.3 Saturation 12

1.5.4 Adiabatic Following Condition 13

Chapter 2 Our Experiment **14**

2.1 The Sodium Slowing Transition 14

2.2 Atomic Beam 17

2.3 The Magnetic Field of the Slower 21

Chapter 3 Numerical Simulation **24**

3.1 The Main Design Ideas 25

3.1.1 Tapered Solenoid versus Mulitiple Coil Zeeman slower 25

3.1.2 Zero Crossing of the Field 26

3.1.3 Concentric Cylinder Design of the Coils 27

3.2 The Simulation 30

3.2.1 Field of a Single Coil 31

3.2.2 Fitting the Desired Field 32

3.3 Results of the Simulation 33

3.3.1 Calculating the Field of the Zeeman Slower 33

3.3.2 Checking the Results of the Simulation 38

Chapter 4 Design of the Coils **42**

4.1 Coil Holder 42

4.2 Winding of the Coils 43

4.3 Comparison between Measurement and Simulation 48

4.4 Manufacturing the Slower Coils 50

Chapter 5 Electronic Regulation **52**

5.1 Current Control Board 52

5.1.1 PI Regulator 54

5.1.2 The Power MOSFET 55

5.1.3 The Pickup Signal 57

5.1.4 Display 58

5.1.5 External interrupt of the current 59

5.1.6 Adjusting a Current Control Board 60

5.2 Temperature Interlock 61

5.2.1 Operation Breakdown of the Temperature Interlock 61
5.2.2 Adjusting a Temperature Interlock Board 63
5.3 Assembly of the Electronics 64
5.3.1 Reference and Supply Voltages 64
5.3.2 Voltage Supplies for the Coils 66
5.4 Problems of the Electronics 66

Chapter 6 The Magnetic Field of the Slower **69**
6.1 Measuring the Magnetic Field 69
6.2 Noise of the Field and Perpendicular Field Components 72

Chapter 7 The Zeeman Slower's Environment **74**
7.1 Thermal Atom Source 74
7.1.1 The Candlestick Oven 74
7.1.2 Collimation of the Atom Beam 75
7.1.3 Gate Valve 76
7.2 The Science Chamber 77

Appendix A Universal and Sodium Specific Constants **78**

Appendix B Eagle Schematics of the Circuit Boards **79**

Bibliography **84**

Vita **86**

Chapter 1

Introduction

1.1 The Concept of Laser Cooling

In the last two decades, a new experimental branch has developed in physics, called *Atom Optics*. This field studies the behavior of atoms interacting with electromagnetic radiation. To perform precision measurements on atoms, it is necessary to create a well defined initial state ideally lacking thermal motion. While those atoms would be at zero temperature, "cold" atoms are atoms very close to zero temperature. For some elements, cooling the atoms down to a temperature close to zero can be achieved by laser cooling. Moreover, in atom optics, one needs the proper tools to manipulate the motion of atoms. In some cases, this tool is provided by lasers, too. The first slowing of atoms flying in an atomic beam was observed in 1982 by Phillips and Metcalf [1], and the first cooling of trapped atoms was done in 1985 by Chu et. al [2].

In this chapter we give a brief introduction to the method of laser cooling including some problems connected to real systems used in experiments, and the limitations of this technique.

Let us consider a two-level atom (ground state $|g\rangle$ and excited state $|e\rangle$) at rest in

the presence of a resonant laser beam, i. e. $\nu_\mathrm{l} = (E^\mathrm{e} - E^\mathrm{g})/(2\,\pi\,\hbar)$, where ν_l is the frequency of the laser, and E^e, E^e are the energies of the atomic ground and excited state respectively. If the atom is in its ground state, it has a high probability to absorb a photon from the laser beam. It is transferred into its excited state. Considering momentum conservation, the atom experiences a recoil (a momentum change by absorbing the photon). The resulting velocity change is

$$\delta v_\mathrm{recoil} = \frac{\hbar\,k}{M}, \tag{1.1}$$

where k is the wave vector of the used laser light ($k = \frac{2\,\pi}{\lambda_\mathrm{l}}$), and M is the mass of the atom.

After a certain time the atom will decay into its ground state by spontaneous emission of a photon. The emitted photon can have arbitrary wave vector and polarization. Thus after many absorption and re-emission cycles, the momentum kick that the atoms receives by re-emitting a photon will average to zero (in zero order approximation), leaving a net force on the atom from the absorption process. This force is called *scattering force* or *radiation pressure force* [3].

Let us now consider the one-dimensional case of a moving atom with velocity v. We assume that the laser beam is resonant in the rest frame of the atom. Thus in the laboratory frame its frequency is shifted by $\delta\nu_\mathrm{l} = \frac{v}{\lambda_\mathrm{l}}$, where λ_l is the wavelength of the used laser light. With respect to the considerations above, the atom will be accelerated for $v \uparrow\uparrow k$, and decelerated for $v \uparrow\downarrow k$, provided that the laser is resonant at all times.

1.2 Doppler Shift

One issue that we briefly mentioned in the last paragraph is the Doppler shift in the case of a moving atom with changing velocity and a laser beam. The Doppler shift is of great importance in laser cooling since it can stop cooling processes if it is

not taken into account, or it can be used in a proper geometry to damp the atomic motion toward a constant velocity, usually chosen to be zero.

Let us consider the same case as in the previous paragraph, but relax the requisite that the laser beam has to be resonant at all times. If the laser beam is resonant at the beginning of our experiment, the change in velocity will lead to a change in the Doppler shift. As the velocity is changed more and more, the atom becomes gradually transparent to the laser. To describe this effect quantitatively, we consider the rate at which photons are scattered out of the laser beam by spontaneous emission. The *scattering rate* γ_p is derived in [3], and is.

$$\gamma_p = \frac{s_0\,\gamma/2}{1 + s_0 + (2\,\delta/\gamma)^2}, \tag{1.2}$$

with $\gamma = 1/\tau$ the natural linewidth, $\delta = \omega_\mathrm{l} - \omega_\mathrm{a}$ the detuning or the difference between the frequencies of the laser and the atomic transition, and s_0 the saturation parameter defined by

$$s_0 = \frac{I}{I_s},$$

with the saturation intensity $I_s = \frac{\pi\,h\,c}{3\lambda^3\,\tau}$. Fig. 1.1 shows the scattering rate γ_p/γ as a function of the detuning δ/γ, both measured in terms of natural linewidths. The saturation parameter is set to $s_0 = 1$*. The graph in Fig. 1.1 shows that for no detuning ($\omega_\mathrm{l} = \omega_\mathrm{a}$) the scattering rate is maximal, and it decreases for increasing detuning. For a detuning $\delta = 3.5\ \gamma$ one gets a scattering rate of $5 \cdot 10^{-2}\,\gamma$, for a detuning of $\delta = 5\ \gamma$ the scattering rate is $5 \cdot 10^{-3}\,\gamma$, and for $\delta = 30\ \gamma$ the scattering rate is $1 \cdot 10^{-3}\,\gamma$.

The graph in Fig. 1.1 has an effect on the interaction between atom and laser, since a changing Doppler shift implies a detuning of the laser in the rest frame of the atom. Below we give a rough, order of magnitude estimate of how many scattering events would make an atom transparent to a laser beam; we assume that a scatter-

*For larger values of s_0 another effect has to be taken into account called *saturation broadening*; see [3].

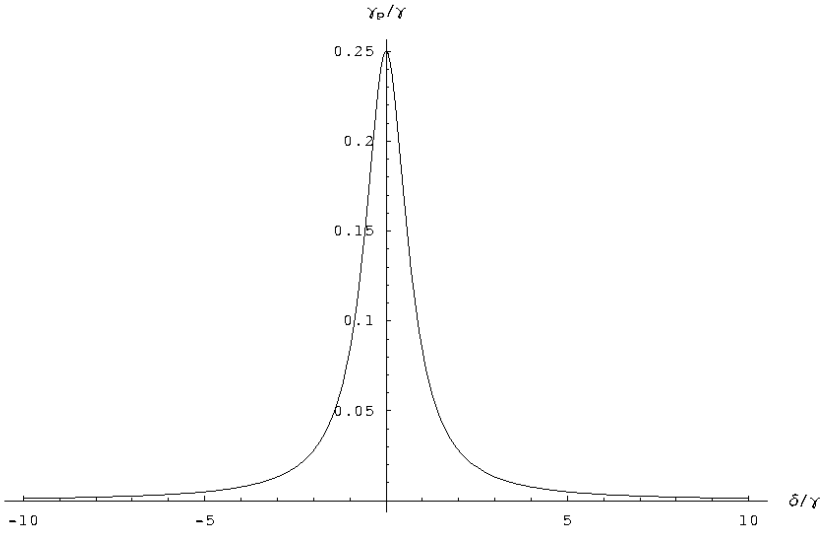

Figure 1.1: Graph of the scattering rate γ_p versus the detuning δ corresponding to eq. (1.2). The saturation parameter is set to $s_0 = 1$.

ing rate of $\gamma_p = 10^{-2}\,\gamma$ can be considered "transparent".

The natural linewidth γ for alkali atoms is on the order of $2\pi\cdot$ 10 MHz, thus a detuning of $3.5 \cdot \gamma$ (corresponding to $\gamma_p = 10^{-2}\,\gamma$) would be on the order of 100 MHz. The laser usually used in laser cooling experiments with alkali atoms have wavelengths of hundreds of nanometers. Hence the velocity change that gives the same frequency shift as the detuning is on the order of $\Delta v = \lambda \cdot \Delta\nu \approx 10\ \frac{\mathrm{m}}{\mathrm{s}}$. The recoil velocities $\delta v_{\mathrm{recoil}}$ are on the order of $10^{-2}\ \frac{\mathrm{m}}{\mathrm{s}}$. That means that an atom would become transparent for the laser beam after roughly 10^3 scattering events.

In some cases, this is used to damp the atomic velocity toward zero. Consider the one-dimensional case of two counter propagating laser beams. Both are detuned slightly to the red of the atomic transition. An atom traveling with velocity v sees the counterpropagating laser detuned to the blue, hence closer to the atomic tran-

sition. As can be seen from Fig. 1.1, the scattering rate increases with smaller detuning. On the other side, the atom sees the copropagating laser further red detuned, leading to an even smaller scattering rate. Thus the probability for absorbing a photon from the counterpropagating beam is higher than the probability to absorb a photon from the copropagating beam. This leads to an effective slowing of the atom. The final velocity of the atom is ideally zero, since at that velocity the probability to absorb a photon is the same for both laser beams.
This method of cooling atoms by counterpropagating beams is called *Optical Molasses* (OM) and is very frequently used. It can be extended to the two- and three-dimensional case by applying laser beams in orthogonal directions. It should be noted that the OM compresses only the velocity distribution, not the spatial distribution.

When working with a single laser beam slowing for instance an atomic beam and not working with a standing wave of light, it is crucial to compensate for the changing Doppler shift, because otherwise the slowing would stop after some scattering events, as we estimated above. One possibility to keep the laser resonant with an atom whose velocity is changing, is to apply a magnetic field. In the next section we will study the effect of a magnetic field on an atom.

1.3 Atoms in a Magnetic Field

The formal treatment of an atom in a magnetic field has to start with its Hamiltonian and from there calculate the energy levels of the atom. A detailed description can be found in [4]. We start with a hydrogen-like atom in the state $|n\, l\, m_l\rangle$, where n denotes the principal quantum number, l is the angular momentum quantum number, and m_l is the magnetic quantum number. The valence electron is in a spin-state noted by $|s\, m_s\rangle$. We couple the spin of the outermost electron $\vec{S}$ with the angular momentum

$\vec{L}$ to calculate the total angular momentum $\vec{J} = \vec{L} + \vec{S}$. Furthermore, we couple the total angular momentum of the electron $\vec{J}$ with the nuclear spin $\vec{I}$ to calculate the total angular momentum of the atom $\vec{F} = \vec{J} + \vec{I}$. The total state of the atom is now $|\alpha\, F\, m_F\rangle$, where α stands for all the quantum numbers that are not given explicitly. F can have the values $|I-j|$, $|I-j|+1$, ..., $I+j-1$, $I+j$, and for a given value of F, m_F can range from $-F$, $-F+1$, ..., $+F$.

In the absence of a magnetic field, all the states with the same value of F are energetically degenerate. This degeneracy is lifted in the presence of a magnetic field. Depending on whether the magnetic interaction in the Hamiltonian is greater or less than the spin-orbit interaction, one distinguishes the cases of (a) strong magnetic fields (the spin-orbit interaction is neglected), (b) Paschen-back effect (the spin-orbit interaction is treated as perturbation), and (c) weak magnetic fields (the magnetic field is treated as a perturbation). We consider here case (c) where the interaction with the magnetic field is small compared with the spin-orbit coupling. The resulting shift in energy is given by

$$\Delta E^{\mathrm{Z}} = g_F\, m_F\, \mathcal{B}_z\, \mu_{\mathrm{B}}, \tag{1.3}$$

with $\mu_{\mathrm{B}} \equiv e\hbar/2m_e c$ the Bohr magneton, $\mathcal{B}_z$ the magnetic field strength in z-direction, m_F the magnetic quantum number, and

$$\begin{aligned} g_F &= g_J \cdot \frac{F(F+1) + J(J+1) - I(I+1)}{2F(F+1)}; \\ g_J &= 1 + \frac{J(J+1) + S(S+1) - L(L+1)}{2J(J+1)}. \end{aligned} \tag{1.4}$$

the Landé factors. For more detailed derivations see [4].

Let us now consider the one-dimensional case of a moving atom in a magnetic field that is shaped so that it is zero at $z = 0$ and increases linearly to both sides (see Fig. 1.2). The magnetic field splits the magnetic sublevels energetically depending

on the exact position. Because of this, an atom at rest would see the laser beam's frequency shifted in its rest frame, depending on the exact position. The parameters can be chosen in such a way that if the atom is located to be right of the magnetic field minimum, it sees the beam incident from the right shifted toward resonance and vice versa. Thus the atom is pushed toward $z = 0$. Moreover, because of the same considerations as above, the atom is slowed down. We just described a one-dimensional *Magneto Optical Trap* (MOT). This scheme can also be easily extended to three dimensions.

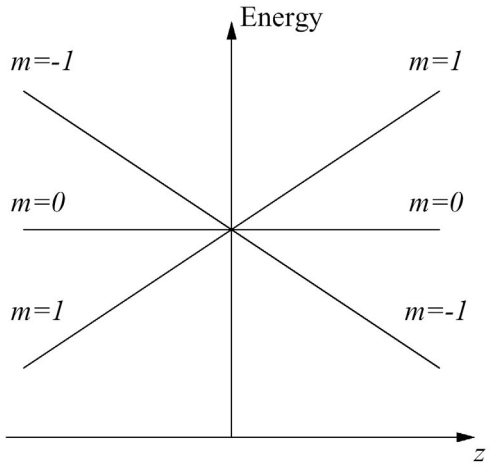

Figure 1.2: Sketch of the spatial dependent energy split of Zeeman sublevels ($F = 1$) in a one-dimensional MOT.

Another possibility for applying a magnetic field is to eliminate the Doppler shift by using the Zeeman shift. The condition for this is

$$\frac{\Delta E^{\mathrm{Z}}(z)}{h} = \frac{v(z)}{\lambda}, \tag{1.5}$$

where ΔE^{Z} is the energy shift due to the magnetic field. The left hand side of eq. (1.5) gives the detuning between the two levels due to the Zeeman shift, the right

hand side gives the detuning due to the Doppler shift. Using eq. (1.3) in eq. (1.5), we get for the magnetic field $\mathcal{B}_z(z)$

$$\mathcal{B}_z(z) = \frac{h \cdot v(z)}{\lambda \cdot \Delta(g_F\, m_F) \cdot \mu_\mathrm{B}}. \tag{1.6}$$

The method of compensating for the Doppler shift by Zeeman shift is frequently used, and a device using this method is called a *Zeeman slower*.

1.4 Real Systems

The discussion so far has most of the time considered a two-level atom. Besides that several approximations were made that need to be considered in more detail now; we will focus on the issues that we need for the discussion of the Zeeman slower later in the text.. This includes the many possible transitions within an atom, and the need for an additional laser (called a "repump" laser) in most cases, as well as a closer look at the behavior of the atoms when reemitting a photon.

1.4.1 Slowing Transition

First of all when dealing with a multi-level atom, one has to take into account that there might be decay channels into states that cannot be excited by the used laser light. To ensure that this is not the case, one usually uses transitions between states of maximal angular momentum and magnetic quantum numbers F and m_F. Let us consider the case of an atom in a ground state $|\alpha,\, \tilde{F},\, \tilde{m_F}\rangle$, where $\tilde{F}$ and $\tilde{m_F}$ are the maximal possible values for a state with the quantum numbers α. This atom is excited with σ_+ polarized light, and thus in the excited state $|\alpha',\, \tilde{F}+1,\, \tilde{m_F}+1\rangle$. Even if an atom was initially in another sublevel, after some cycling transitions it will have the ground state we described above, because its magnetic quantum number is increased by one in every excitation, but does not necessarily decrease in every decay. Because of dipole selection rules, the excited state can only decay back into

the first ground state. We have formed a closed transition. To avoid excitations in other states that might be close in frequency to the slowing transition, those states can be shifted in frequency by applying a magnetic field, and compensate for that by detuning the laser respectively.
The need to find a slowing transition that has not many concurrence transitions, limits the number of elements that can be slowed by lasers.

1.4.2 Repumping

Although the slowing transition described above is closed, there are some regimes where atoms can access a state from where they cannot be excited again.
Let us consider an atomic beam leaving an oven (see section 2.2), and let us assume that there exist two hyperfine ground levels with values $|g,\ F = 1\rangle$ and $|g,\ F = 2\rangle$ (see for instance Fig. 2.1 on page 15). It can be easily calculated that at temperatures where one creates a thermal beam, the atoms are distributed equally among the magnetic sublevels of the two ground states[†]. However, the slowing laser interacts only with atoms in the hyperfine state with maximal quantum number $|g,\ F = 2\rangle$. Thus, the population of the other state would be lost; this state is called a *dark state*. To include the population of the $|g,\ F = 1\rangle$ state, a laser beam tuned to the $|g,\ F = 2\rangle \longrightarrow |e,\ F = 3\rangle$ transition is applied. From here, the atoms has a nonzero probability to decay into the "right" ground state $|g,\ F = 2\rangle$. Such a laser is called an *optical repump* laser, since it pumps the atom into a state from where it can decay into the right ground state and hence contribute to the slowing.

Let us now consider the slowing cycle as above in the absence of a magnetic field. As long as the light of the laser beam is completely circularly polarized, there is no possibility of exciting an atom into another state than the described one. However,

[†]Assuming a temperature of several hundred Kelvin and thermal Boltzmann distribution

in experiments polarization is never perfect, and some fraction of the light might be linearly polarized. In the absence of a magnetic field, this light can lead to a transition $|\alpha, \tilde{F}\rangle \longrightarrow |\alpha', \tilde{F}\rangle$, from where it can decay into a state like $|\alpha, \tilde{F}-1\rangle$. This state is called a *dark state*, since an atom in this state does not see the laser light any more. Although the channels concurrent to the slowing cycle are considerably weaker, and the fraction of linearly polarized light can be kept low, this can be a substantial loss mechanism due to the usually large number (10^4) of transitions. This can be avoided by applying a repump laser as described above.

1.4.3 Transverse Heating

When we described the slowing cycle in section 1.1 we said that the recoils from the reemission of a photon average to zero. But since the recoil processes are discrete and separate in time, the atom undergoes a random walk while absorbing resonant photons and reemitting photons.

The result of this random walk is that atoms experience a nonzero velocity change from the reemission process. The velocity can be split into a component parallel to the moving direction, and two components perpendicular to the moving direction. Here we are mainly interested in the perpendicular velocity components, since they heat the atom in the plane perpendicular to the z-axis. From the theory of random walk it can be derived (see [5]) that the mean velocity spread in one dimension of the three-dimensional problem scales like

$$\overline{\Delta v_\perp} \propto \sqrt{\frac{N}{3}} \cdot \delta v_{\mathrm{recoil}}, \tag{1.7}$$

where N is the number of reemission events.

1.5 Limitations

In this section we present some issues that impose limits on the experimental realization of laser cooling. Those issues include the competition between a high number of atoms and a good vacuum, the fundamental limits of laser cooling, the saturation at high intensities, and the so-called adiabatic following condition.

1.5.1 Number of Atoms versus Background Pressure

In experiments with cold atoms, there is always a little thermal motion left due to the nonzero temperature. This motion can be detected as noise in the experimental data. To improve the signal to noise ratio, it is necessary to maximize the number of atoms.

In many experimental setups atoms are collected from the background pressure in a MOT and further cooled down. To increase the number of atoms, one has to increase the pressure in the system. However, the untrapped atoms in the background vapor can collide with the cooled atoms and by those collisions transfer energy to the cooled atoms. This leads to a heating of the sample and limits the cooling process. Moreover, those collisions can lead to a loss of atoms if the transferred energy is high enough for the formerly cooled atom to leave the trap.

There are several schemes to overcome this problem. The first possible scheme is to use two MOTs. The first MOT collects atoms from a high background pressure. Those atoms are transferred to the second MOT region, the pressure in which is considerably smaller than in the first MOT region. By repeatedly transferring atoms, a high number of atoms is accumulated in the second MOT at a low pressure.

Another possible experimental setup is to load a MOT with an atomic beam that has been slowed by laser cooling. The pressure in the MOT region can be much

smaller than in the region of the thermal source. This is of great importance, since it permits a high number of trapped atoms in an environment of high vacuum. The issue of slowing an atomic beam will be discussed in more detail in the next chapter, because it is the slowing method that we use in the new experiment.

1.5.2 Cooling Limit

Laser cooling – for instance in a MOT – is not able to cool a sample of gas to arbitrary low temperatures. One reason for this is the random walk that the atoms undergo while being slowed. A limit is reached when the diffusive pressure due to the random walk equals the radiation pressure. The lowest velocities that can be reached are on the order of several recoils.

An even more fundamental limit is given by the quantization of the momentum transfer. Even if an atom could be brought to zero velocity, it is hard to ensure that it will not absorb photons any more. However, this can be overcome by certain schemes; one possible method can be found in [6].

1.5.3 Saturation

In the discussion of the scattering rate eq. (1.2), we did not discuss the saturation parameter s_0. Lets consider a two level atom with a laser tuned to resonance, $\delta = 0$ at a very high intensity:

$$I \gg I_s \equiv \frac{\pi\, h\, c}{3\, \lambda^3\, \tau} \Longrightarrow s_0 \gg 0.$$

It can be shown [3] that in this case the population is equally distributed between the ground and the excited state. Moreover, in this limit the scattering rate (1.2) becomes

$$\lim_{s_0 \gg 1} \gamma_p = \frac{\gamma}{2}. \tag{1.8}$$

That means in other words that the time of a complete cycle is in saturation $2 \cdot \tau$, with τ the lifetime of the excited state. This finite time for a cycle cannot be shortened by higher laser intensity. This problem leads to another limit called adiabatic following.

1.5.4 Adiabatic Following Condition

Lets consider the case of compensating for Doppler shift by Zeeman shift (section 1.3). In eq. (1.6) the exact function $v(z)$ can be rewritten as a function of the radiation pressure force exerted on the atom $F_{\text{rad}} = m \cdot a(z)$. where $v(z) = \int_{z_0}^{z} a(z')\, dz'$. Lets further assume the case of σ_+ polarized light, a slowing transition between states of maximal F values, and a decelerating atom. The magnetic field for this case can be calculated using eq. (1.6) and choosing a function $v(z)$.

To save space and to build a small Zeeman slower, one could try to increase the average acceleration a on the atoms arbitrarily high, and vary the field over a huge range of magnetic field strengths in a very small spatial interval, hence creating a large magnetic field gradient. However, the considerations in section 1.5.2 show that this is not possible, but that a limit is imposed on this kind of slowing (see [7]).

Since one slowing cycle has a finite lifetime of $2 \cdot \tau$, and the corresponding velocity change is δv_{recoil}, the largest possible acceleration that can be imposed onto the atoms is

$$a_{\max} = \frac{\delta v_{\text{recoil}}}{2\,\tau}. \tag{1.9}$$

If the magnetic field in our case is increased so that the atoms had to slow down with an even higher acceleration, they will drop from the slowing process and are lost.

Chapter 2

Our Experiment

The purpose of the experiment, that the described Zeeman slower is a part of, is to eventually create a Bose-Einstein Condensate (BEC) and perform high precision experiments with this relatively new state of matter. In this chapter we describe the specific properties of our experiment that lead to the design of the Zeeman slower we use. We will take into account the issues that were mentioned in the last chapter. We use sodium in our experiment. As an alkali metal it is easy to create a vapor, and sodium is amenable to laser cooling techniques.

2.1 The Sodium Slowing Transition

The slowing transition we use is the D_2 transition $3\ ^2S_{\frac{1}{2}}|F = 2,\ m_F = 2\rangle \longrightarrow 3\ ^2P_{\frac{3}{2}}|F = 3,\ m_F = 3\rangle$, as shown in Fig. 2.1 in red. This transition has a wavelength of 589 nm and can be excited by a dye laser.

Moreover we apply a repump beam to the transition $3\ ^2S_{\frac{1}{2}}|F = 1\rangle \longrightarrow 3\ ^2P_{\frac{3}{2}}|F = 2\rangle$. Due to the shape of the magnetic field in our Zeeman slower there exists a region of zero magnetic field; in this region the magnetic sublevels are degenerate, and atoms can be lost as described in section 1.4.2 by exciting them with a small fraction of

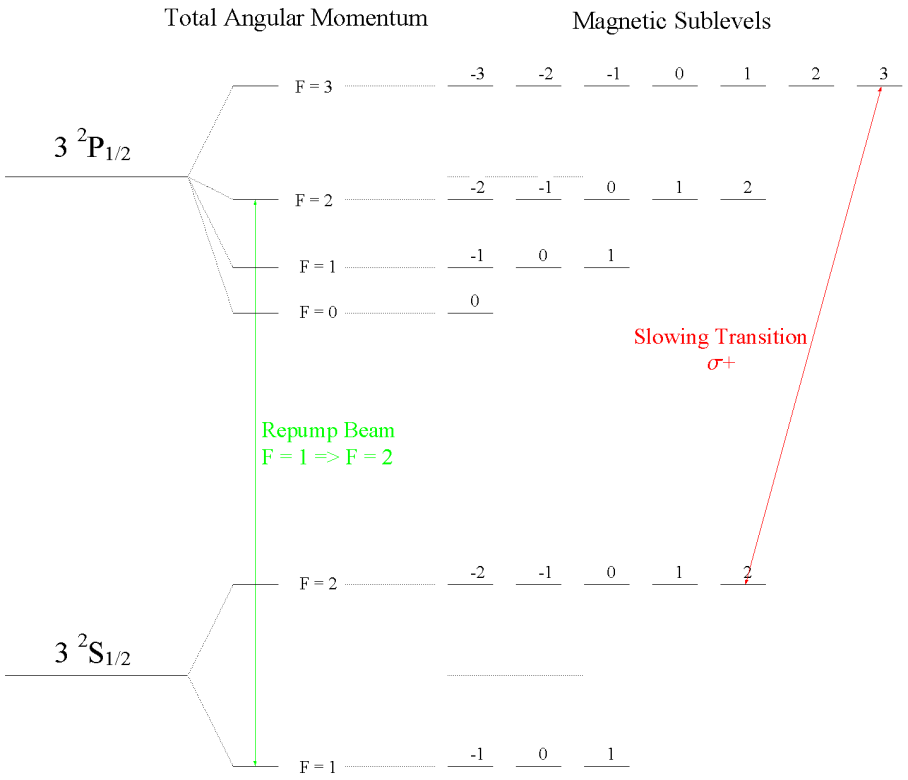

Figure 2.1: Scheme of the ground ($3\ ^2S_{\frac{1}{2}}$) and first excited ($3\ ^2P_{\frac{3}{2}}$) energy level in the sodium atom (I = 3/2)(Not to scale). The corresponding line is called the D_2 line, and the transition has a wavelength of 589 nm. The hyperfine structure splitting of energy levels with different total angular momentum quantum numbers F is shown as well as the different magnetic sublevels with quantum numbers m_F that split energetically in a magnetic field. The slowing transition between states of extreme quantum numbers $|F = 2, m_F = 2\rangle \longrightarrow |F = 3, m_F = 3\rangle$ is shown in red, and the repump transition $F = 1 \longrightarrow F = 2$ that applies in case of magnetic sublevel degeneracy is shown in green.

linearly polarized light from the $3\ ^2S_{\frac{1}{2}}|F=2\rangle$ to the excited state $3\ ^2P_{\frac{3}{2}}|F=2\rangle$. From there they can decay into the $3\ ^2S_{\frac{1}{2}}|F=2\rangle$ ground state, a dark state. Although the strength of this channel is significantly less than the slowing channel (about 1/3 the strength of the main slowing transition), and the light fraction that can contribute to this excitation is typically just a few percent (lets assume 1% for estimation purposes), we get a probability of 1/300 that an atom is excited into the "wrong" state;

To see whether this could cause a problem, we have to know how many cycling transitions an atom usually has to undergo. For sodium the recoil velocity is $\delta v_{\text{recoil}} = 2.9$ cm/s, and a reasonable velocity interval over that the atom has to be slowed, is from 1000 m/s to 0 m/s. This gives a total of about 35 000 cycling transitions. Considering this high number of more than 30 000 scattering events, a probability to lose an atom every 300 scattering events would be a substantial loss mechanism. This can be compensated by an applied repump laser, because an atom that is re-excited into the $3\ ^2P_{\frac{3}{2}}|F=2\rangle$ can later decay into the $3\ ^2S_{\frac{1}{2}}|F=2\rangle$ ground state, and be slowed again.

The repump is also crucial in a second region. As we saw (see section 1.4.2) the atoms are uniformly distributed among all the hyperfine ground states when they leave the oven. However, the slowing beam only affects atoms in the $|F=2\rangle$ ground state. A repump tuned to the $3\ ^2S_{\frac{1}{2}}|F=1\rangle \longrightarrow 3\ ^2P_{\frac{3}{2}}|F=2\rangle$ transition increases the output of the Zeeman slower, because it pumps the atoms into the "right" ground state and makes them visible for the slowing beam.

Since the detuning of the slowing beam compensates for the velocity of the atoms at $\mathcal{B}_z = 0$ (about 400 m/s in our experiment), and the repump in this region has to have the same detuning, it cannot be used to optically pump the atoms right after the oven before entering the magnetic field of the Zeeman slower. For the faster atoms right after the oven, the repump can be created by adding sidebands

to laser beams that are resonant to the D_2 line. Those laser beams are used in a two-dimensional optical molasses configuration after the oven to decrease the velocity of the atoms transverse to the axis of the atomic beam. The sidebands perform transverse optical pumping.

2.2 Atomic Beam

The last step in the process of creating a BEC is evaporative cooling. In this cooling method the fastest atoms can leave the trap, and after rethermalization of the sample, its mean temperature has decreased. The loss in this process is generally very high (usually more than 99% of the atoms are lost during evaporation); to have still enough atoms to perform experiments on, one has to start out with a very high number. In a former experiment an approach with a double MOT configuration was unsuccessful at trapping more than 10^7 atoms.

As mentioned in section 1.5.1, one possibility for loading a MOT quickly with many slow atoms, is to decelerate atoms flying in a collimated atomic beam with a counterpropagating laser beam. To create such an atomic beam, sodium has to be heated to a high temperature (such as 500 K), and from the ensemble a small, well collimated fraction is extracted.

We describe the thermal atom source in our experiment in section 7.1.1, and consider below the question of which fraction of atoms can be slowed from an atomic beam, given a certain temperature in the oven and a maximal initial velocity of the atoms that can be slowed. We assume a final velocity of zero for estimation purposes, although in the experiments the atoms drop from the slowing process with about 10 to 30 m/s. From other experiments with sodium [1, 8] we know that initial velocities $v_\mathrm{i} \leq 1000\ \frac{\mathrm{m}}{\mathrm{s}}$ can be slowed. We choose $v_\mathrm{i} = 1000\ \frac{\mathrm{m}}{\mathrm{s}}$ and $v_\mathrm{i} = 800\ \frac{\mathrm{m}}{\mathrm{s}}$ as examples for calculating the fraction of atoms that can be slowed by a Zeeman slower.

Velocity Distribution of the Atomic Beam

If one wants to calculate the fraction of slowed atoms depending on the velocity for a certain temperature, one has to take into account that the velocity distribution in a three-dimensional gas $f^{\mathrm{3D}}(v)$ differs from the distribution in an atomic beam $f^{\mathrm{beam}}(v_z)$ [3]:

$$f^{\mathrm{3d}}(v) = \sqrt{\frac{2}{\pi}} \cdot \frac{v^2}{\tilde{v}^3} \cdot \exp\left[-\frac{v^2}{2\,\tilde{v}^2}\right] \tag{2.1}$$

$$f^{\mathrm{beam}}(v_z) = \frac{v_z^3}{2\,\tilde{v}^4} \cdot \exp\left[-\frac{v_z^2}{2\,\tilde{v}^2}\right], \tag{2.2}$$

with $\tilde{v} = \sqrt{\frac{k_{\mathrm{B}}\,T}{m}}$. In Fig. 2.2 the velocity distribution in an atomic beam is shown for T = 500 K (blue line) together with the Maxwell-Boltzmann velocity distribution in a three-dimensional gas at the same temperature (dashed line). The red line marks the velocity $v = 800\ \frac{\mathrm{m}}{\mathrm{s}}$. The maximum of the distribution is before the line, thus we expect in this case to slow more than half of the atoms from the source. In Fig. 2.3,

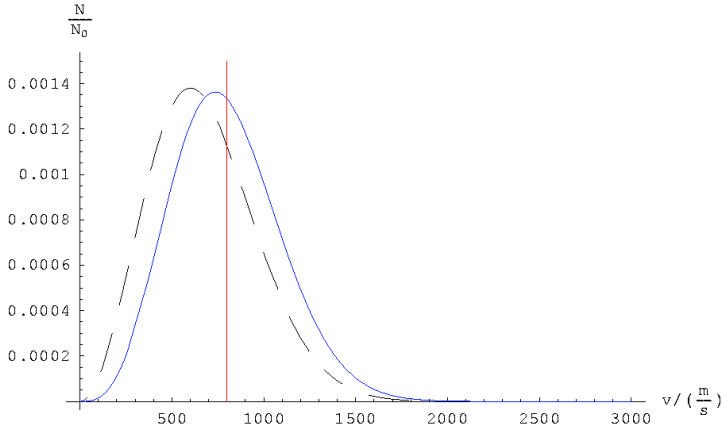

Figure 2.2: Velocity distribution for an atomic beam at T = 500 K (blue line) together with the Maxwell-Boltzmann distribution for a three-dimensional gas. The red line is at $v = 800\frac{\mathrm{m}}{\mathrm{s}}$.

we show a graph of the fraction of atoms that are slowed down depending on the initial velocity v_i, resulting from integrating equations (2.1) and (2.2). Calculating the fraction of atoms with a velocity $v \leq v'$, one gets for $v_1' = 1000\,\frac{\mathrm{m}}{\mathrm{s}}$ and $v_2' = 800\,\frac{\mathrm{m}}{\mathrm{s}}$ respectively:

$$\left.\frac{N^{\mathrm{3D}}}{N_0}\right|_{v_1'} = 0.86 \quad ; \qquad \left.\frac{N^{\mathrm{beam}}}{N_0}\right|_{v_1'} = 0.76;$$
$$\left.\frac{N^{\mathrm{3D}}}{N_0}\right|_{v_2'} = 0.68 \quad ; \qquad \left.\frac{N^{\mathrm{beam}}}{N_0}\right|_{v_2'} = 0.53;$$

For higher initial slowing velocities the gain in the number of atoms becomes less (the first derivative decreases monotonically when $N/N_0 > 0.5$). In the case of sodium

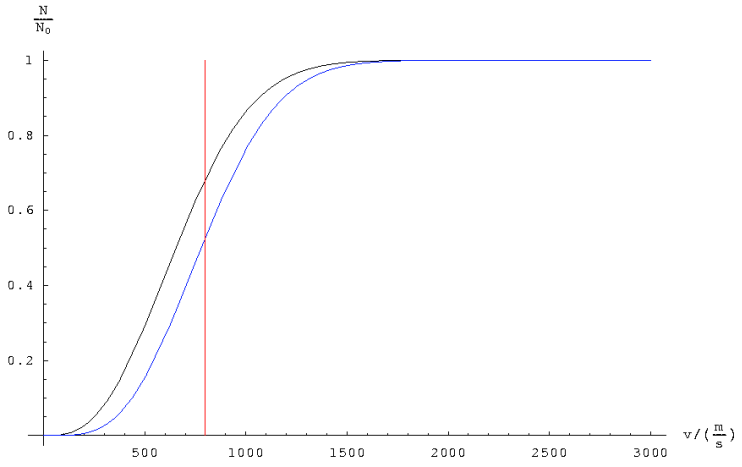

Figure 2.3: Graph of the fraction of slowed atoms depending on the initial slowing velocity. The red line corresponds to $v = 800\ \frac{\mathrm{m}}{\mathrm{s}}$

atoms, about $30,000$ slowing transitions are necessary to slow an atom down from $v_\mathrm{i} \approx 10^3\ \frac{\mathrm{m}}{\mathrm{s}}$ to $v_\mathrm{f} \approx 10\ \frac{\mathrm{m}}{\mathrm{s}}$. The time of flight for the fastest atoms ($v_\mathrm{i} = 10^3\ \frac{\mathrm{m}}{\mathrm{s}}$) is about 2 ms, and 100 ms for the ones flying with $v = 10\ \frac{\mathrm{m}}{\mathrm{s}}$

A MOT can capture and cool atoms in a final velocity range of $v_\mathrm{f} = 10$ to $30\ \frac{\mathrm{m}}{\mathrm{s}}$. Considering the large velocity difference $v_\mathrm{i} - v_\mathrm{f}$, one has to take into account the

drastically changing Doppler shift. As we showed before (see section 1.2), atoms would become transparent after a few thousand transitions. Doing the same calculations with the values for sodium (see Appendix A), we get for sodium about 3000 scattering events before the atom sees the laser beam detuned by three linewidths. On the other hand, many atoms have to undergo more than 3000 cycles (up to 30 000), so that in our case we have to compensate for the Doppler shift.
This could be done by changing the laser frequency, so that the laser is always resonant to one bunch of atoms, but this would lead to a pulsed source of slow atoms. However, in our case it is more favorable to use a continuous source of slow atoms to quickly load the MOT with a large number of atoms.
Using a Zeeman slower, we estimate from research groups with similar geometry [8] a flux of about $10^{10}\ \frac{\text{atoms}}{\text{s}}$ into a solid angle of $5 \cdot 10^{-6}$ sr.

Another issue that has to be discussed at this point, is the effect of transverse heating due to the random walk of the atoms during the slowing process. This leads to an increase in the divergence of the beam. This has to be compared with the intrinsic divergence of the atomic beam. From other groups with similar geometry, we can estimate that atoms with a z-component of the velocity of 1000 $\frac{\text{m}}{\text{s}}$ have a mean velocity in the perpendicular direction of $\overline{v_\perp} \approx 22\ \frac{\text{m}}{\text{s}}$ (see section 7.1.2).
From eq. (1.7) for atoms with the same initial z-component of the velocity we can estimate the mean velocity gain in one dimension of to be:

$$\overline{\Delta v_\perp} = \sqrt{\frac{N}{3}} \cdot \delta v_{\text{recoil}} \approx 2.9\ \frac{\text{m}}{\text{s}}.$$

This is one order of magnitude smaller than the intrinsic divergence of the beam and thus negligible in our case.

2.3 The Magnetic Field of the Slower

To calculate the shape of the magnetic field $\mathcal{B}_z(z)$ that one needs to compensate for the Doppler shift, we start out from equation (1.6). For the sodium D_2 transition we get

$$\Delta(g_F\, m_F) = g_F^e\, m_F^e - g_F^g\, m_F^g = 1, \tag{2.3}$$

with $g_F^e = \frac{2}{3},\ m_F^e = 3,\ g_F^g = \frac{1}{2}$, and $m_F^g = 2$.

The last free parameter is the function $v(z)$. We assume constant deceleration $v(z) = \sqrt{v_\mathrm{i}^2 - 2\,a\,z}$. The field in the slower is thus given by

$$\mathcal{B}_z = \frac{h}{\mu_\mathrm{B}} \left(\Delta_0 + \frac{1}{\lambda} \sqrt{v_\mathrm{i}^2 - 2\,a\,z} \right); \tag{2.4}$$

where we added a detuning Δ_0 of the laser. The acceleration is chosen to be $a = 0.5 \cdot a_\mathrm{max}$, with $a_\mathrm{max} = -9.4 \cdot 10^7\ \frac{\mathrm{cm}}{\mathrm{s}}$ for sodium. This ensures that the adiabatic following condition is not violated, even if the magnetic field given by (2.4) shows small deviations from its ideal value.

A graph of the ideal shape of the magnetic field is shown in Fig. 2.4 for $\Delta v_z = 990$ m/s, $a = 0.5\ a_\mathrm{max}$, and $\Delta_0 = 0MHz$. The shape and absolute position of the magnetic field can be influenced by three parameters:

1. The difference between initial (v_i) and final (v_f) velocity (Δv).
2. The value of the constant acceleration a.
3. The value of the detuning Δ of the laser frequency.

Assuming that in every case both other values are fixed, a change in a parameter results in the following change of the magnetic field.

1. A change in Δv leads to a change in the difference between magnetic field maximum and minimum ($\Delta\mathcal{B}_z = \mathcal{B}_z^\mathrm{max} - \mathcal{B}_z^\mathrm{min}$).

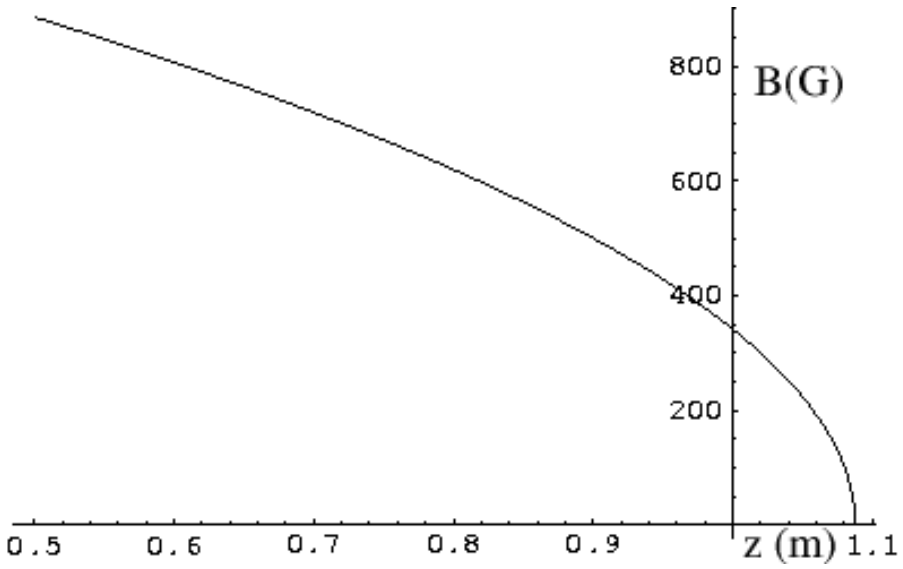

Figure 2.4: Graph of the magnetic field calculated by Eq. 2.4; this magnetic field provides a Zeeman splitting on the atoms that compensates for the Doppler Shift at any spatial point for sodium atoms and a laser frequency tuned to the Na D2 transition. The used parameters are $\Delta v_z = 990$ m/s, $a = 0.5\ a_{\max}$, and $\Delta_0 = 0MHz$.

2. A change in the acceleration a leads to a stretching or compressing of the field along the z-axis. For a larger value of a the slowing occurs over a shorter distance, hence the field is compressed, and vice versa.

3. A change in the detuning results in a shift of the magnetic field along the $\mathcal{B}_z$-axis. A detuning to the red translates to a shift to higher magnetic fields*.

These three flexible parameters allow for modification of the field to what is desired for the experiment.

The problems that lead to a certain choice of a parameter will be described in Chapter 3.

*assuming σ_+ polarized laser light

Chapter 3

Numerical Simulation

Most Zeeman slowers use a tapered solenoid to create the spatially varying field by a spatially varying number of windings. This design does not allow for independent adjustment of parameters, such as the acceleration a, the detuning, or the difference between the maximum and minimum slowable velocities.

In the case of several identically wound coils with a spatially varying current, most parameters are still adjustable in a certain range, even when the slower is already in operation. Moreover, in case of an accident, most likely only one or a few of the coils would be damaged and could be replaced easily – in a good design they could even be rewound in place, avoiding a break of the vacuum system. The flexibility of the modular Zeeman slower, consisting of many separate coils, gave rise to the decision to go with this design.
The numerical simulation for the design of the Zeeman slower was done using Mathematica and provided the dimensions for the coils that had to be built as well as the currents that are needed to get a field as described in eq. (2.4). In the following chapter, a sketch of the program is given, together with the main aspects of optimizing the Zeeman slower. At last, the results of the final simulation are pre-

sented leading to the design that we eventually use, and the behavior of this design concerning noise is investigated.

3.1 The Main Design Ideas

There are basically three main issues that influenced the design of the Zeeman slower and helped choose proper values for the parameters introduced in Section 2.3 as well as the geometric parameters of the solenoid (like length, radius, etc.).
These issues are smoothness of the magnetic field, power dissipation, and weight of the slower. Moreover it advantageous to have a design that is flexible and allows for changes even when the experiment is already set up.

3.1.1 Tapered Solenoid versus Mulitiple Coil Zeeman slower

As shown in Eq. 2.4, the main goal of the Zeeman slower is to provide a spatially varying magnetic field. The field created by a long solenoid with current flowing through it, is proportional to the number of windings and the magnitude of the current:

$$\mathcal{B}_z \propto N \cdot \mathcal{I}.$$

This shows that either the number of windings has to be varying with z, or the current $\mathcal{I}$ has to change with the spatial point.

In the first case, usually a long tapered solenoid is used, where a single long wire is wound with a spatially varying number of windings.
The disadvantage is that once wound, the used parameters cannot be changed independently anymore. The bias field and thus the detuning cannot be easily changed without changing the range of slowed velocities, nor can the velocity of the extracted atoms be influenced without adding other components.

In the case of a changing current, several coils are wound identically and the currents through them are different. The disadvantage of this design is that with a similar workload the smoothness of the field is worse than in the case of a tapered solenoid. The smoothness of the field increases with the numbers of steps in windings or current respectively, i. e. how well the ideal field is rastered. Whereas in the case of a tapered solenoid on a length of one meter usually more than twenty steps are used, we use only thirteen. This of course results in deviations from the ideal field, but operating far enough from the maximum acceleration, this has no effect on the slowing process, as will be shown later (see section 6.1).
The main advantage of this design is that in principle all parameters can be changed, including the initial slowed velocity, the extraction velocity, and the detuning of the laser frequency. The great flexibility achieved with this design was the main argument to use it in the experiment.

3.1.2 Zero Crossing of the Field

Calculating the field for a slower that slows down atoms from 1000 $\frac{\mathrm{m}}{\mathrm{s}}$ to about 10 $\frac{\mathrm{m}}{\mathrm{s}}$* with several coil geometries using the unmodified equation (2.4) showed a huge power dissipation, since the magnetic field has to vary from approx. 1200 Gauss to approx. 400 Gauss. Even after optimization of these values, the Zeeman slower would require an intense cooling.
One possible method to decrease the magnetic field strength and thus lower the dissipated power, is to subtract a constant value $\delta\mathcal{B}_z$ from each point of the magnetic field, shifting the field along the $\mathcal{B}_z$-axis and change the detuning. In the case where the lowest power dissipation occurs, the field varies symmetrically from $+|\tilde{\mathcal{B}}_z|$ to

*For an oven temperature of 500 K the most probable velocity of Sodium atoms is at $v_{\mathrm{mp}} = \sqrt{\frac{3\,k_B\,T}{M}} \approx 736\,\frac{\mathrm{m}}{\mathrm{s}}$; i. e. 76% of the atoms are slowed. For a initial slowing velocity of 800 $\frac{\mathrm{m}}{\mathrm{s}}$ it would be 53%, see section 2.2, Fig. 2.2 and 2.3.

$-|\tilde{\mathcal{B}}_z|$. This design that includes a zero crossing of the magnetic field is called a *Spin Flip Zeeman slower*, since in the rest frame of the magnetic field the spin of the atoms flip at the point of the zero crossing.
There are two problems connected to the design of a Spin Flip slower:

- In the region of the zero crossing, the magnetic sublevels of the $F = 2$ state are not separated in frequency any more so that atoms can get lost from the slowing when they are excited by π-polarized light and decay into a dark state. As described in Section 1.4.2 this can be overcome by applying a proper laser beam.

- At the point where the magnetic field along the z-axis is zero, the atoms could lose their polarization in the absence of other magnetic fields. But as described in [9], this problem can be solved by introducing a weak magnetic field perpendicular to the z-axis of the slower.

The big advantage of low power dissipation gives rise to the decision to use this design in our experiment.

3.1.3 Concentric Cylinder Design of the Coils

By introducing the zero crossing of the magnetic field, the power dissipation can be considerably decreased; nevertheless, cooling is still an issue. Besides the amount of heat that is dissipated, it is important to see, how this heat is conducted from the core of the coil to the surface of the holder, and whether water cooling is necessary to take the heat away, or if air cooling is sufficient.
A rough estimation shows that a single copper cylinder with two copper plates is not suited, since the heat is transferred quickly only from the regions near the copper plates. The more layers of wire are wound onto the cylinder, the less wire is in contact with the copper.

On the other hand it is not reasonable to decrease the number of windings and increase the current through the coil instead. Though the magnetic field scales linearly with both:

$$\mathcal{B}_z \propto N \cdot \mathcal{I},$$

the dissipated power scales quadratically with the current:

$$P = U \cdot \mathcal{I} = R \cdot \mathcal{I}^2.$$

Thus regarding low power dissipation, it is more favorable to use more windings and less current to create a certain field.

The first approach to solve the heat transfer problem, was to introduce more copper plates parallel to the holding plates (see Fig. 3.1). But this design showed shorts after winding, because on the edges of the new copper plates, the high pressure due to the many layers of wire above, injured the insulation and shorted the wire and the holder.

Another approach was to introduce a second, bigger cylinder that the wire would be wound onto (see Fig. 3.2). A rough worst case estimate of the heat transfer shows that this design can deal with the dissipated power.

Heat Transfer in the Concentric Cylinder Case We assume that all the heat is dissipated in the middle of the innermost cylinder. For the other cylinder, the area over which the heat is transferred, increases, whereas the other parameters stay fixed; hence this case of the innermost cylinder is the worst case. Furthermore we assume a cylinder with an outer diameter of 7 cm and a length of 7 cm. The resulting area of the cylinder's cross section is 6.67cm^2. Assuming a temperature difference of $\Delta T = 80$ K (outside 20°C, inside 100°C) the maximal heat current H (see Fig. 3.3) is:

$$H = k \cdot A \cdot \frac{\Delta T}{\Delta x}, \tag{3.1}$$

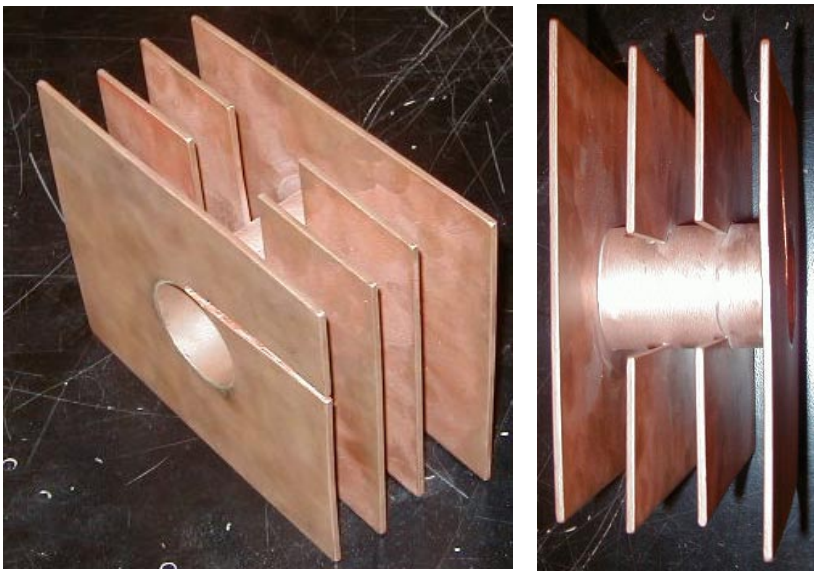

Figure 3.1: Pictures of the first coil design. This design was not used, because there is a high danger of wire being shorted to the copper at the edges of the inner copper plates

Figure 3.2: Layout of the coil holder in the concentric cylinder case. The design is described in detail in section 4.1

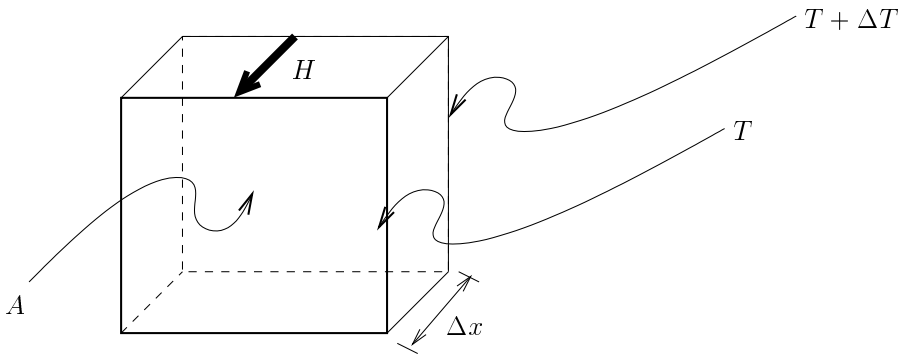

Figure 3.3: For Eq. 3.1: Heat transfer through a box with area A over a distance Δx

where k is the thermal conductivity of the material. With the given numbers we get for copper ($k = 4\ \frac{\mathrm{W}}{\mathrm{cm \cdot K}}$): $H = 610$ W, and for brass ($k = 1.2\ \frac{\mathrm{W}}{\mathrm{cm \cdot K}}$): $H = 180$ W; this is far more power than in one coil will be dissipated, thus the heat created in the core of the coil will be transferred outside, and the temperature in the coil will not exceed a temperature of roughly 100°C.

3.2 The Simulation

In order to determine the right coil geometry — including length and number of coils, diameters of the cylinders, number of windings, and gauge of the wire — the magnetic fields for several such geometries were simulated. Here I give a brief introduction to the simulation followed by promising results.

The numerical simulation is written in the language Mathematica. Starting from (a) the magnetic field of a single coil the geometry of which has to be given, and (b) the desired magnetic field, the currents that need to be run through the different coils are calculated by fitting.

The relative error between ideal and simulated field is calculated and the spatially

varying acceleration is compared with the limit of adiabatic following (see Section 1.5.4). The program gives the power dissipation of each coil and the total dissipation. After that, noise is imposed onto the calculated values for the currents, and the behavior of the magnetic field regarding the adiabatic following is calculated.

3.2.1 Field of a Single Coil

Only the magnetic field along the z-axis is important for the slowing process. Therefore an analytical expression may be used to calculate the magnetic field at a point z along the axis of a single wire loop located in the xy plane with diameter d sitting at location z_0 carrying a current I (see Fig. 3.4):

$$\mathcal{B}_z(z, I, d, z_0) = \frac{\mu_0 \cdot I \cdot d^2}{2 \cdot (d^2 + (z - z_0)^2)^{\frac{2}{3}}}, \tag{3.2}$$

where all quantities are in SI units. When calculating the field of a coil, the pro-

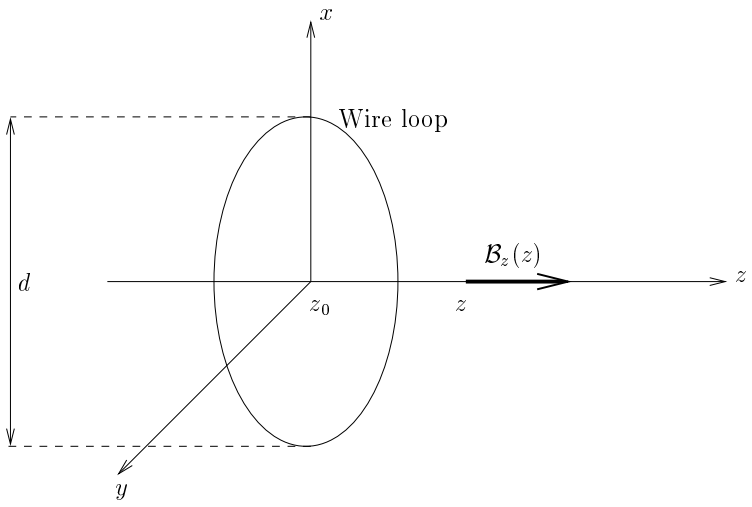

Figure 3.4: For Eq. (3.2).

gram simply adds the contributions of individual wire loops, taking into account the number of windings in the horizontal and vertical directions, as well as the wire

gauge and the starting point z_0 of the first wire loop. These parameters are given as variables to a function called "f".

Since the coil consists of two concentric cylinders, the function $\mathit{field}(z) = f_{\text{inner}}(z) + f_{\text{outer}}(z)$ is used for further calculations, where $f_{\text{inner}}(z)$ stands for the function "f" for the inner cylinder and $f_{\text{outer}}(z)$ for the outer cylinder.

From the specified geometry, the function *field* can be used to calculate the total length of wire for each coil. Given the resistance per unit length for the gauge of wire that we are using, the total resistance of the wire can then be calculated.

The program calculates the magnetic field from one coil with a current of $I = 1\ A$ over a total range of 3 m centered near zero with a resolution of 1 mm. This range is necessary to accurately calculate field values over the entire size of the Zeeman slower. The resolution of 1 mm is sufficient because all of the field coils and their spacing are much larger than 1 mm[†].

From this calculation an interpolating function is generated (using the default polynomial of third order in Mathematica), that matches the 1 mm data well and is easier to manipulate than the function *field* itself.

3.2.2 Fitting the Desired Field

We would like to generate a field that is very close to that described by Eq. 2.4. The value for the initial atomic velocity is chosen to be $v_{\text{i}} = 800\ \frac{\text{m}}{\text{s}}$. The acceleration parameter is set to $a = 0.50 \cdot a_{\max}$, which corresponds to a slower length of $13 \cdot 7$ cm $= 91$ cm. To estimate which fraction of the oven output is slowed by this parameter set, one has to integrate the velocity distribution of the atoms in the beam (see section 2.2).

This ideal field is shifted such that the absolute value of the maximum and minimum values of the magnetic field strength are equal. After that, another shift is imposed,

[†]The fields produced by these coils are also smooth over this length scale.

so that the Doppler Shift at the zero crossing point matches the detuning of the laser of Δ_0 = -600 MHz[‡].

We model the desired field as this shifted function, evaluated with 1 mm resolution over a range of 1 m. The interpolated field of thirteen coils sitting next to each other is fitted to this array using the standard Mathematica `Fit` routine. The field of a single coil was calculated with a current of $I = 1$ A and this current is a separable parameter (as can be seen in Eq. 3.2). The desired currents are thus returned as fitting parameters that create the optimal magnetic field for the given coil geometry.

3.3 Results of the Simulation

In the following section, we present the results of the numerical simulation that led to the design of the Zeeman slower coils. Running several simulations with different geometries, this geometry gave the best compromise with respect to smoothness of the field, power dissipation, and weight of the slower.

3.3.1 Calculating the Field of the Zeeman Slower

Geometry of the Individual Coil

We use a coil consisting of two concentric cylinders. The first has an outer diameter of 3.5 cm, the second 4.8 cm.[§]. We use 18 AWG (gauge) wire and wind 50 windings in one layer. The nominal diameter of the bare wire is 1.02 mm. However, because of the insulation thickness and winding imperfections, we use 1.224 mm in the simulation. Six layers are wound onto the inner cylinder (with a total of about 300 windings), and eight onto the outer (400 windings total).

Using 18 gauge wire is a compromise for low power dissipation at increased weight

[‡]This value is used because it can be achieved by double passing a 260 MHz Isomet Acousto Optic Modulator (AOM) that is operated at 300 MHz.

[§]These are standard size brass pipes with a wall thickness of 0.125 inches.

of the slower. As described in sec. 3.1.3 the power dissipation for a certain magnetic field decreases with increasing wire diameter. But with larger wire diameter, the weight of the slower increases. By choosing 18 gauge we could design an air-cooled slower that weighs (only) about 70 kg.

A plot of the interpolated data of the field of one of those coils is shown in Fig. 3.5.

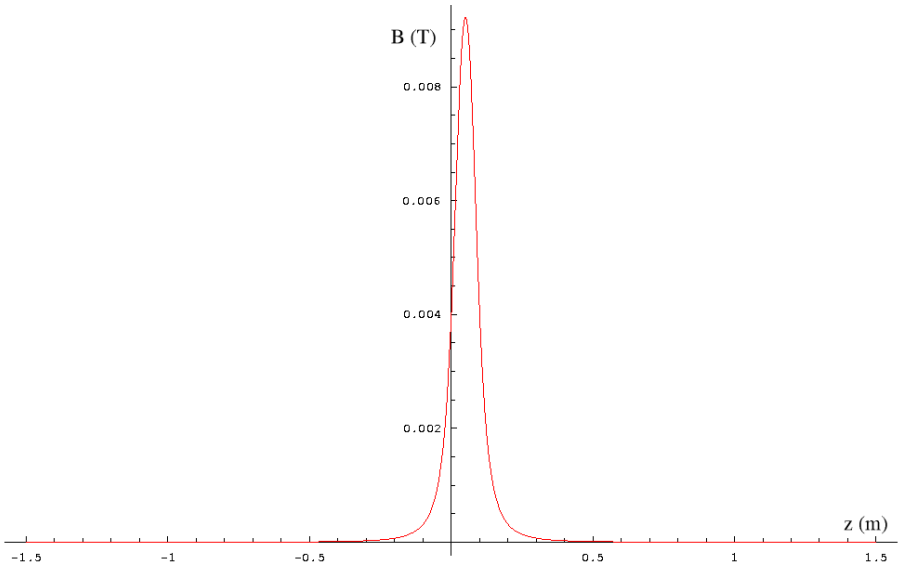

Figure 3.5: Simulated shape of the magnetic field produced by one coil consisting of two concentric cylinders.

Calculating the Currents

As described in Section 3.2.2, the ideal field is shifted, so that it runs from about +500 G to -500 G, slowing atoms from 800 $\frac{\mathrm{m}}{\mathrm{s}}$ to 10 $\frac{\mathrm{m}}{\mathrm{s}}$. The value for the extraction velocity of the atoms is adjustable, because the last coil works as an extraction coil providing a defined end of the slowing process.

The zero crossing can be found in the last third of the slower. A plot of the ideal field

is given in Fig. 3.6. Twelve of the coils are used to fit the ideal field from Fig. 3.6,

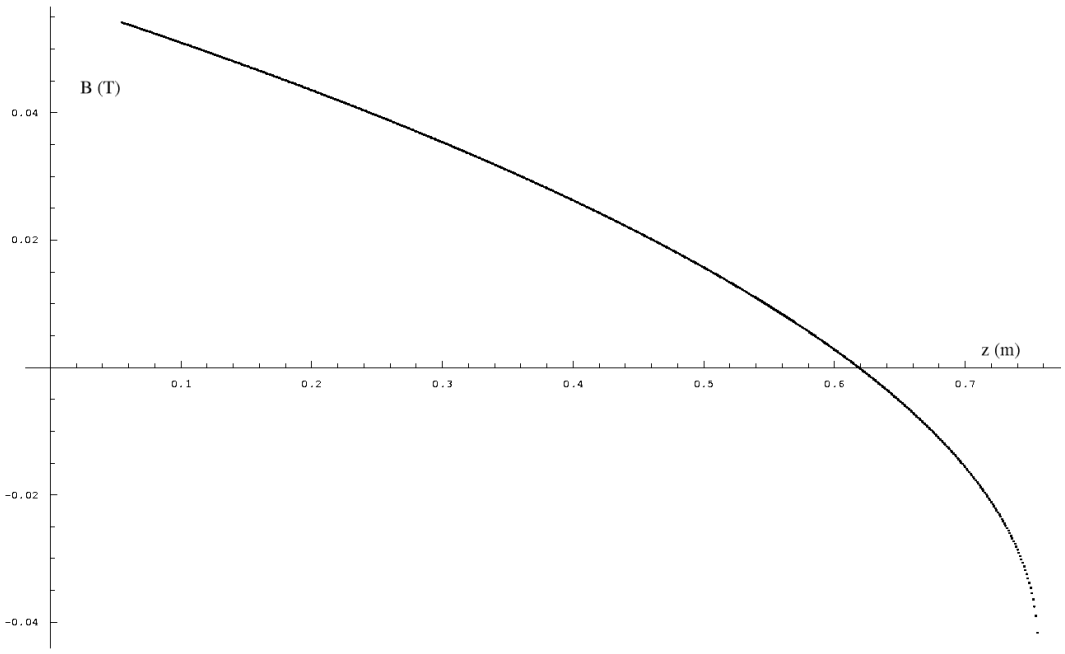

Figure 3.6: Shape of the magnetic field following Eq. 2.4, but shifted to have roughly the same absolute values for the maximal and minimal magnetic field, and shifted to have a detuning of 600 MHz

returning the currents as coefficients for each interpolating function. The current of the last coil is intended to be set manually to adjust the extraction velocity. A table with the finalized currents together with the power dissipated in each coil is given in Tab. 3.1, and a graph of the simulated field together with the ideal field is presented in Fig. 3.7.

# coil	Current/A	Power/W
1	4.64	106
2	3.44	58
3	3.12	48
4	2.68	36
5	2.28	26
6	1.83	16
7	1.34	9
8	0.79	3
9	0.18	1
10	-0.63	2
11	-1.22	7
12	-4.87	117
13	1.00	5

Table 3.1: Table with the calculated currents for the Zeeman slower coils, where coil #1 is on the beginning of the Zeeman slower where the fast atoms enter. The currents in coils # 12 and # 13 were set manually and can be used to adjust the extraction velocity of the atoms. The total power dissipated in the Zeeman slower is about 430 W; in recent designs of tapered solenoids the power dissipation is uasually around 1 kW, but can be up to 3 kW.

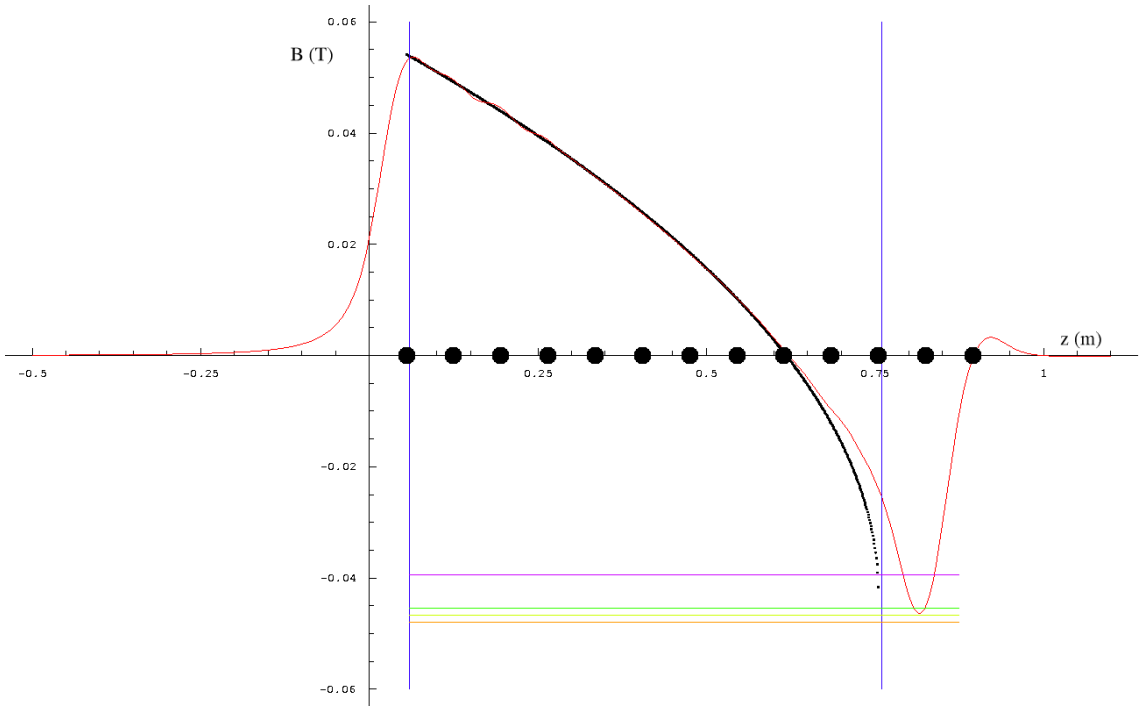

Figure 3.7: Simulated magnetic field using parameters of Table 3.1 (red) line and ideal field (black) of the Zeeman slower. The colored horizontal lines give the magnetic field at which the atoms when extracted have a velocity of 80 $\frac{\text{m}}{\text{s}}$, 30 $\frac{\text{m}}{\text{s}}$, 20 $\frac{\text{m}}{\text{s}}$, and 10 $\frac{\text{m}}{\text{s}}$ (from top to bottom). The big dots on the z-axis mark the positions of the coil centers. The bump on the right end of the slower is due to the extraction coil. The vertical blue lines mark the interval in which the fields of the individual coils were fitted to the ideal field.

3.3.2 Checking the Results of the Simulation

The relative difference between the ideal and the numerically calculated field is determined with the formula

$$\frac{\Delta \mathcal{B}_z}{\mathcal{B}_z^0} = \frac{\mathcal{B}_z - \mathcal{B}_z^0}{\mathcal{B}_z^0}. \tag{3.3}$$

A graph of the resulting function is given in Fig. 3.8. To see whether there is any danger of violating the condition of adiabatic following at some point in the slower, the field derivative $\frac{\partial \mathcal{B}_z}{\partial z}$ is calculated and plotted for the maximal acceleration $a_{\max}$ and the simulated field. Both graphs are shown in Fig. 3.9. As soon as the field derivative of the simulated field (blue line) comes into the region above the adiabatic following limit (red line), atoms no longer participate in the slowing process. (As long as the blue line is below the red, the slowing is expected to work.)

Simulating Noise

To see how the simulated field behaves when noise is added to the currents, a "noise current ΔI" is added to the ideal currents from table 3.1. In calculating the worst case, this noise current is alternately added and subtracted, so that the difference in current between two neighbor coils is $2 \cdot \Delta I$. The noise current was set to several values between 30 mA and 100 mA. Figures of the simulated field and the relative difference are shown in Fig. 3.10.

In none of the investigated cases was the condition of adiabatic following violated, although the smoothness of the field became considerably worse.

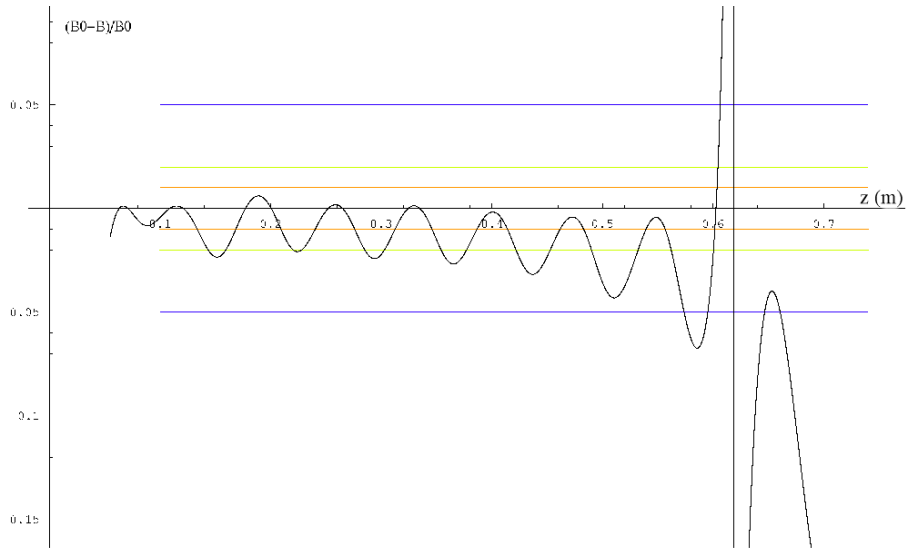

Figure 3.8: Graph of the relative difference between ideal and simulated magnetic field of the slower. The divergence at the last third of the slower is due to the zero crossing of the field (division by zero). The colored lines give the 1% (orange), 2% (green), and 5% (blue) levels of relative deviation from the magnetic field $\frac{\mathcal{B}_z - \mathcal{B}_z^0}{\mathcal{B}_z^0}$

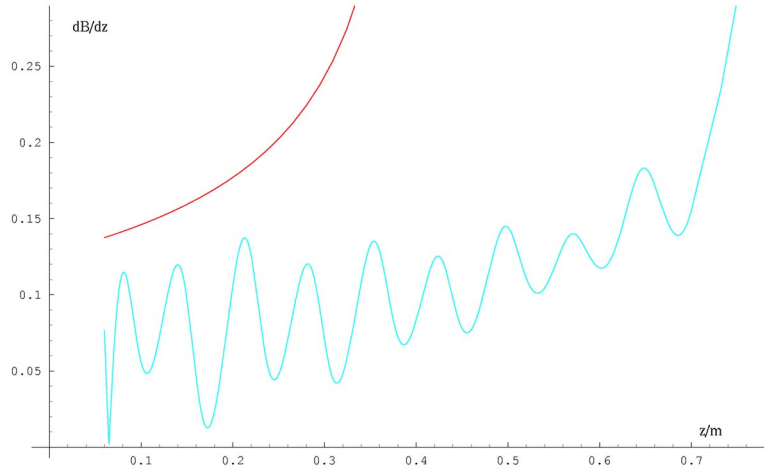

Figure 3.9: Gradients of the ideal magnetic field with $a = a_{\max}$ (red line) and the simulated magnetic field (blue line); as long as the blue line stays under the red line the adiabatic following condition is not violated.

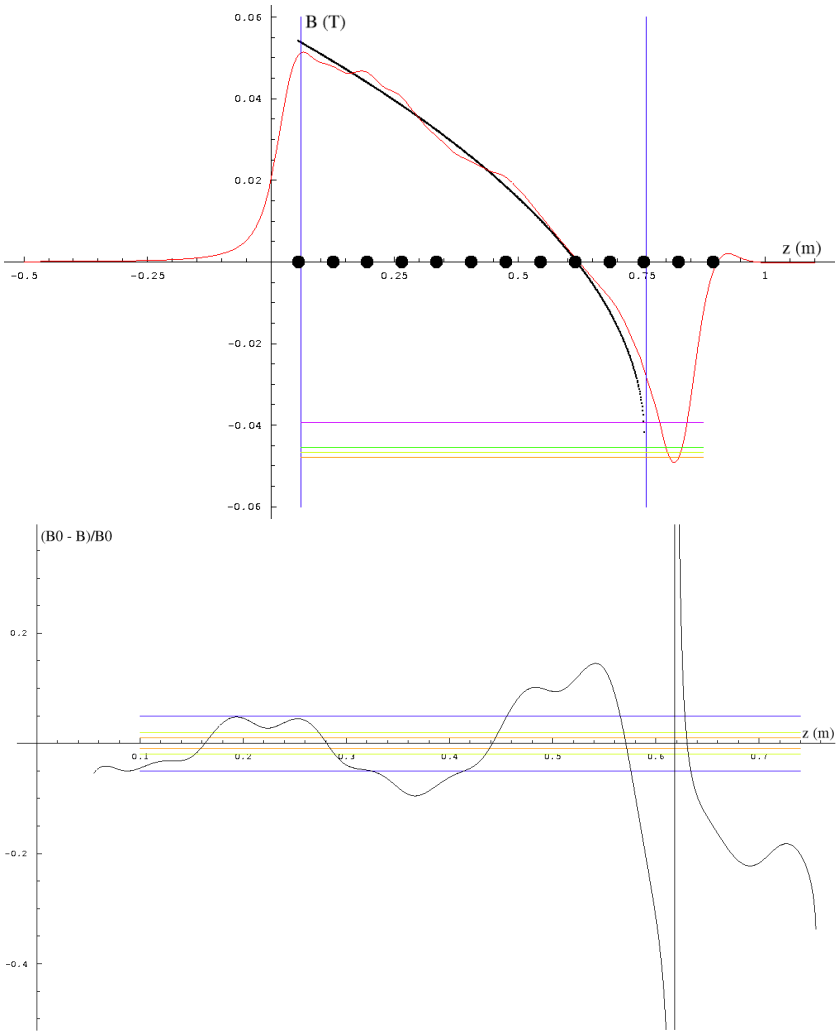

Figure 3.10: Simulation with the same geometrical parameters for the coils as in Fig. 3.7 and 3.8, but with added noise of 100 mA per coil; the noise was added and subtracted alternately. In the top graph the simulated field is shown, in the bottom graph the relative difference. Even in this case, the adiabatic following condition holds.

Chapter 4

Design of the Coils

In the following chapter we describe how the actual coils were designed and built using the geometrical numbers gained from the simulation. This includes: (a) designing the holder, (b) building, winding and testing of a prototype, and (c) making technical drawings to have the coils made in the machine shop, and winding those.

4.1 Coil Holder

The most reasonable numbers from the simulation were two concentric cylinders of length 6.4 cm. The inner cylinder has an inner diameter of 2.5 inches (= 6.35 cm), and the outer has an inner diameter of 3.5 inches (= 8.89 cm). Both have a wall thickness of 0.125 inches = 0.3175 cm.

The problem was how to design a holder that allowed for winding those cylinders separately and assembling the coil afterward, yet still providing enough structural stability to have separate coils. For cooling purposes we chose to have copper plates at both ends of the cylinders to allow for good heat transfer away from the wire. Since the heat transfer from copper to air increases with the area of the copper, the plates were designed rather large (19 cm $\cdot$ 19 cm), with a thickness of 0.125 inches

= 0.3175 cm.

To hold the concentric cylinders in place, about 1 mm deep grooves were milled into the copper plates, so that the cylinders would fit snugly into these grooves. In the middle of each plate, a circular hole with diameter of 2.375 inches = 6.0325 cm was cut. Through this hole an aluminum pipe with a slightly smaller outer diameter fits that carries the coils. Supporting this aluminum pipe and the vacuum pipe independently avoids putting any pressure from the Zeeman slower onto the vacuum pipe, and helps centering both with respect to each other.

As the shallow grooves could only prevent the cylinders from sliding around, on each corner of the copper plates there are eye bolts in which springs can be hooked. This design ensures enough stability so that one coil can be handled easily..

On one side of the copper plate a slit with an opening angle of 25°, vertex in the center, was cut into the copper. This fulfilled two purposes. One, air could be blown directly over the wire through the slits if needed, and two, it helped in feeding through the wire from the inner cylinder to the edge of the copper plate, where the wire connections are located.

The wire connectors are simply aluminum plates (1 cm · 2 cm) that have been wrapped with Dupont Kapton film® (500 HN, 0.005 inches thick, fixed with Kapton film 0.001 inches with 0.002 inches adhesive on one side) to avoid the possibility of a short at this point. These plates are screwed to the copper plate at one end, thereby pressing the wires against the copper that had been also protected by Kapton.

The technical drawings of this design can be found in Fig. 4.1 and 4.2.

Images of the built prototype can be seen in Fig. 4.3.

4.2 Winding of the Coils

As wire for the coils we chose 18 gauge Phelps Dodge Poly-Thermaleze Tough Wire®. The wire has Thermal Class 220 (20,000 hours lifetime at 226°C), and

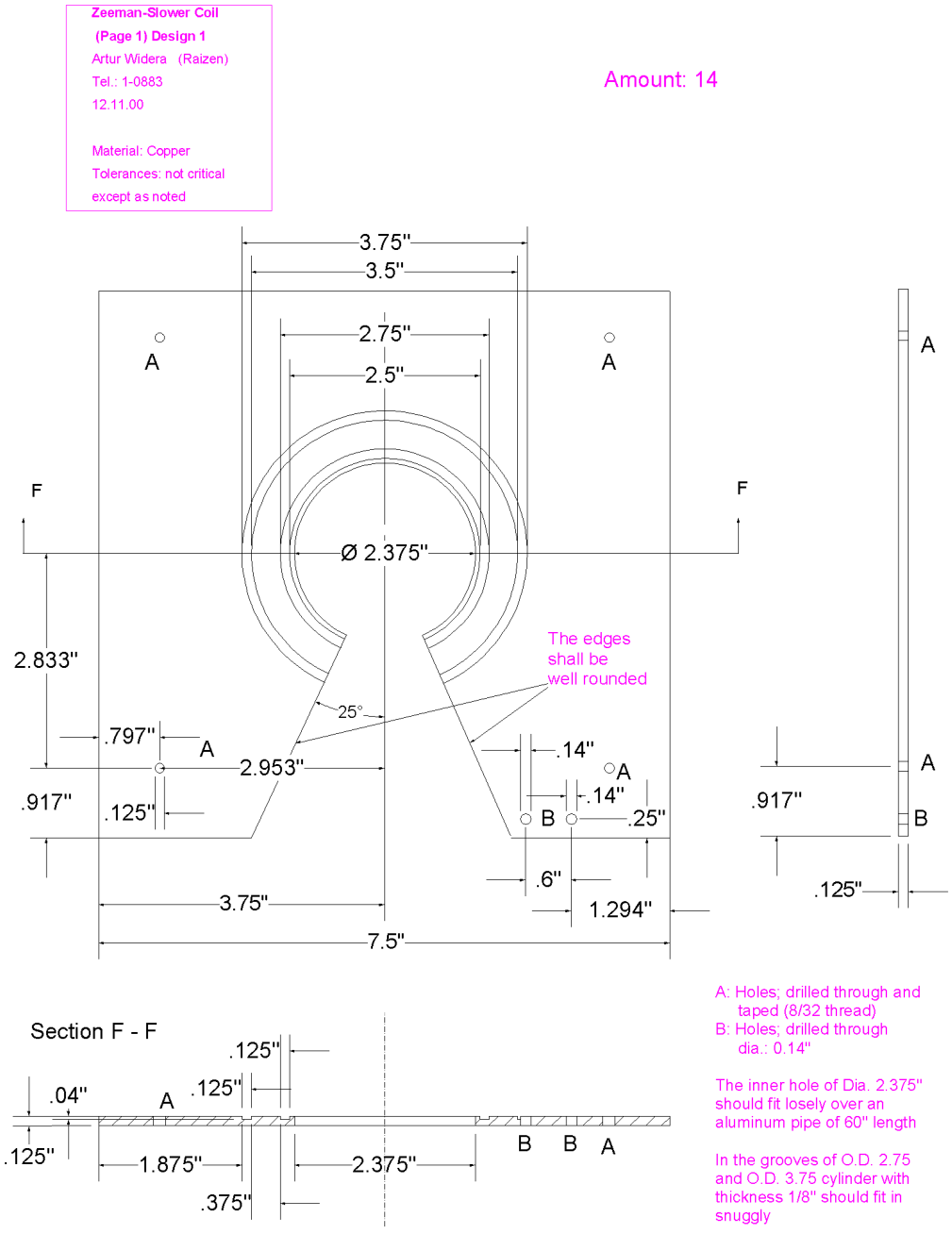

Figure 4.1: Technical drawing of the copper plate with tapped holes for the connection of the magnetic wire. In addition, fourteen plates were manufactured without those holes.

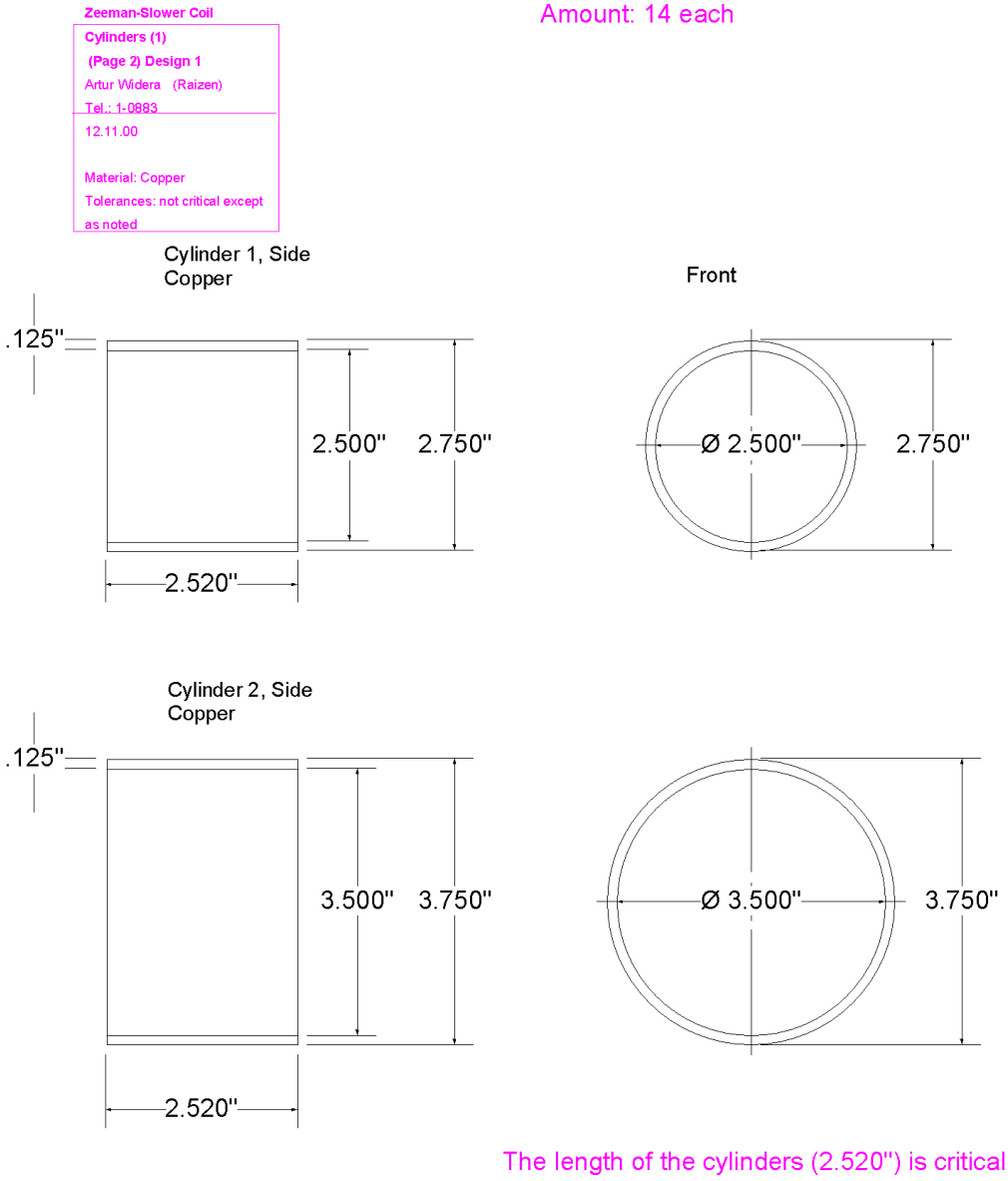

Figure 4.2: Technical drawing of the cylinders onto which the wire was wound. The diameters are standard sizes, the length however was a critical size since both cylinders should fit between the copper plates equally well to conduct heat.

Figure 4.3: The pictures show the built prototype with the geometry used in the simulation. The pictures show the principle idea (upper left), closer looks at the grooves and the fixed cylinders (upper right and lower left), and the idea of holding the Zeeman slower structure with an aluminum pipe.

it is insulated with multiple coatings of polyester and polyamide Imide.
This wire was chosen because it can operate at high temperatures, is backable up to 200°C, and is optimized to resist scratches at the same time.

The coils were wound on a lathe. The copper plates were not used as brackets for the cylinders since the danger of injuring the insulation with the copper edge was too great.
Instead, for each cylinder size a pair of round brackets was machined from Teflon (for the smaller cylinder) and aluminum (for the bigger cylinder). The cylinders fit into these brackets approximately as deep as they will fit later in the grooves (see Fig. 4.4). To prevent the wire from springing off the cylinder being transferred from

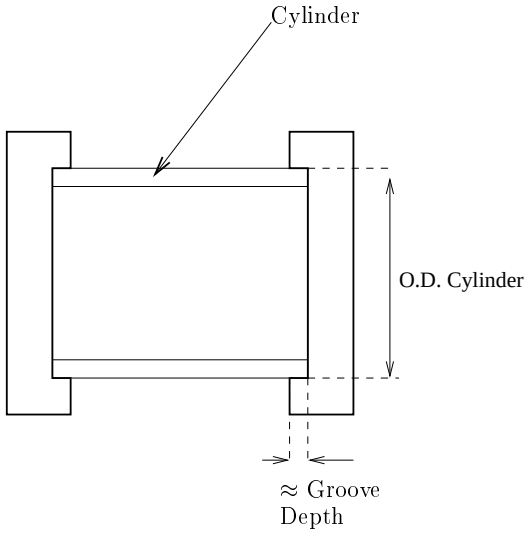

Figure 4.4: Schematics of the brackets used to wind the Zeeman slower coils.

the brackets to the copper plates, at the end of each row glue was applied to some points at the end of the layer. The glue is RTV 108 "Silicone Rubber Adhesive Sealant" by GE Silicones, and can withstand temperatures up to 200°C without

changing its properties.

To prevent the wire from being glued to the bracket, four or five strips of thin Kapton® Film (0.001 inches thick, 0.5 inches wide, with 0.002 inches adhesive on one side) were layed on top of the cylinder parallel to the axis (see Fig. 4.5), so that the Kapton came to lay between bracket and wire. After winding, the two ends of the Kapton strips were knotted and put under tension while the glue was curing. Pictures of the brackets that were used are shown in Fig. 4.6. A picture of two

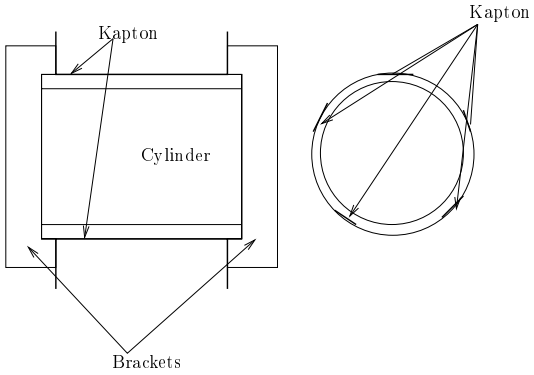

Figure 4.5: Positioning of the Kapton stripes on the cylinders

concentric cylinders wound and mounted between copper plates can also be seen in Fig. 4.6.

4.3 Comparison between Measurement and Simulation

To see whether the field of a single coil was commensurate to the field calculated by the simulation, a prototype coil was wound, connected, and the magnetic field was characterized.

A plot with both the simulated field and the measured field can be found in Fig. 4.7. As can be seen from Fig. 4.7, the magnetic fields do not match perfectly. This is due to the fact that the simulation calculates with a perfect space filling, whereas

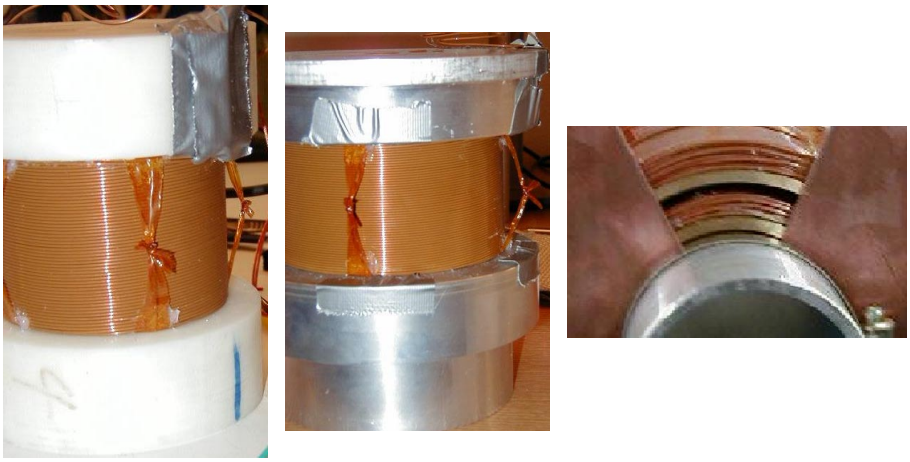

Figure 4.6: Picture of the brackets that were used to wind the Zeeman slower Coils. The Teflon brackets are for the smaller cylinder, the aluminum brackets for the larger cylinder. Over the wire the Kapton film that held the wire together can be seen. Right picture: Two cylinders wound with 18 gauge wire and mounted between two copper plates. The space between the two cylinders helps to cool the wire while the slower is in operation.

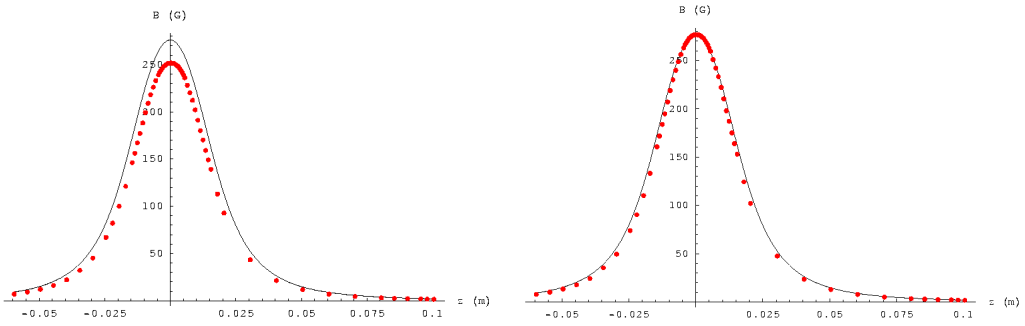

Figure 4.7: Comparison of the magnetic field of the prototype coil with the simulation. In the left graph the measured magnetic field strengths (red dots) are shown together with the simulated magnetic field (black line) without any adjustment. In the right graph, the measured fields are multiplied by a factor of 1.1.

coil itself has wire crossings, holes and spaces between the layers. The ratio of the calculated to the measured field strengths is approximately 1.1, thus by scaling the measurement with this factor, the measured field shape matches the simulation well. A graph of the scaled field together with the simulated field can be found in Fig. 4.7.

The important point in this investigation is that the measured field has the same shape as the simulated one because the shape determines to what degree the ideal slowing field from Eq. 2.4 can be approximated by the single coil fields.

4.4 Manufacturing the Slower Coils

Having verified that the chosen design provides the kind of field that the simulation predicts, technical drawings were made so that the coil holders could be made in the machine shop. The drawings are given in Fig. 4.1 and Fig. 4.2.

With the same method that has been introduced in Section 4.2, fourteen coils were wound. In Table 4.1 the numbers of windings of each coil is given. Into the windings of the inner cylinders of coils # 13 and # 14, a thermocouple Type K is wound to monitor the temperature. This thermocouple can be connected to the temperature interlock device described in section 5.2. These coils will sit at positions 1 and 12 (see Table 3.1) with currents of I = 4.64 A and I = -4.87 A respectively.

Some pictures of the finished Zeeman slower can be seen in Fig. 4.8

# coil	# outer cylinder	# inner cylinder
I	425	320
II	425	310
III	426	323
IV	425	325
V	426	325
VI	425	325
VII	425	320
VIII	422	325
IX	430	320
X	431	321
XI	430	323
XII	433	326
XIII	433	321
XIV	423	321

Table 4.1: Table with the numbers of windings on each coil. The roman enumeration is scribed into the copper plate of the corresponding coil.

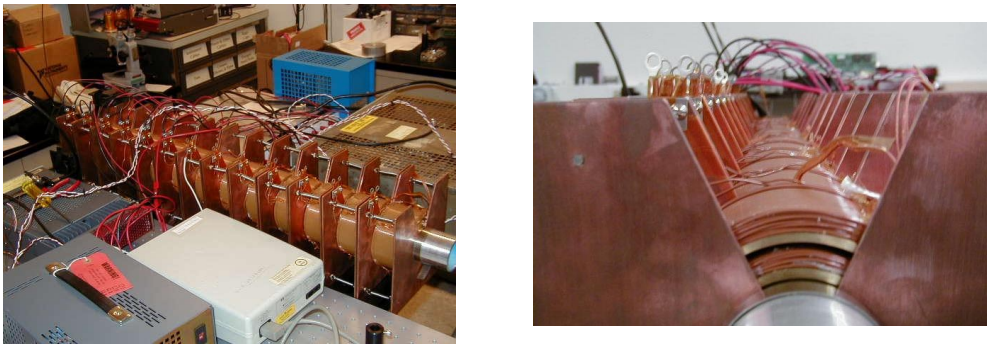

Figure 4.8: Pictures of the finished Zeeman slower being tested. The right picture shows an enlargement of the two concentric cylinders.

Chapter 5

Electronic Regulation

The electronic regulation of the Zeeman slower consists of two parts: One is the regulation of the current through each coil, the other is a temperature interlock. This is read out from a Type K thermocouple and interrupts the current through the corresponding coil and its neighbor coils when the temperature extends some preset value. In the following chapter those two boards are introduced and their assembly is described. The board layouts were created with the computer program EAGLE and are presented in Appendix B. On both boards the supply voltages of all operational amplifiers are coupled to ground over capacitors with a capacitance of C = 0.1 μF to avoid unwanted oscillations.

5.1 Current Control Board

The schematics of the regulator for one coil can be seen in Fig. 5.1. The current through each coil is controlled by one of those boards and can be adjusted separately. In the following section, the current control board is divided into these segments

- The PI* Regulator

*PI stands for proportional integration, see [10] and section 5.1.1

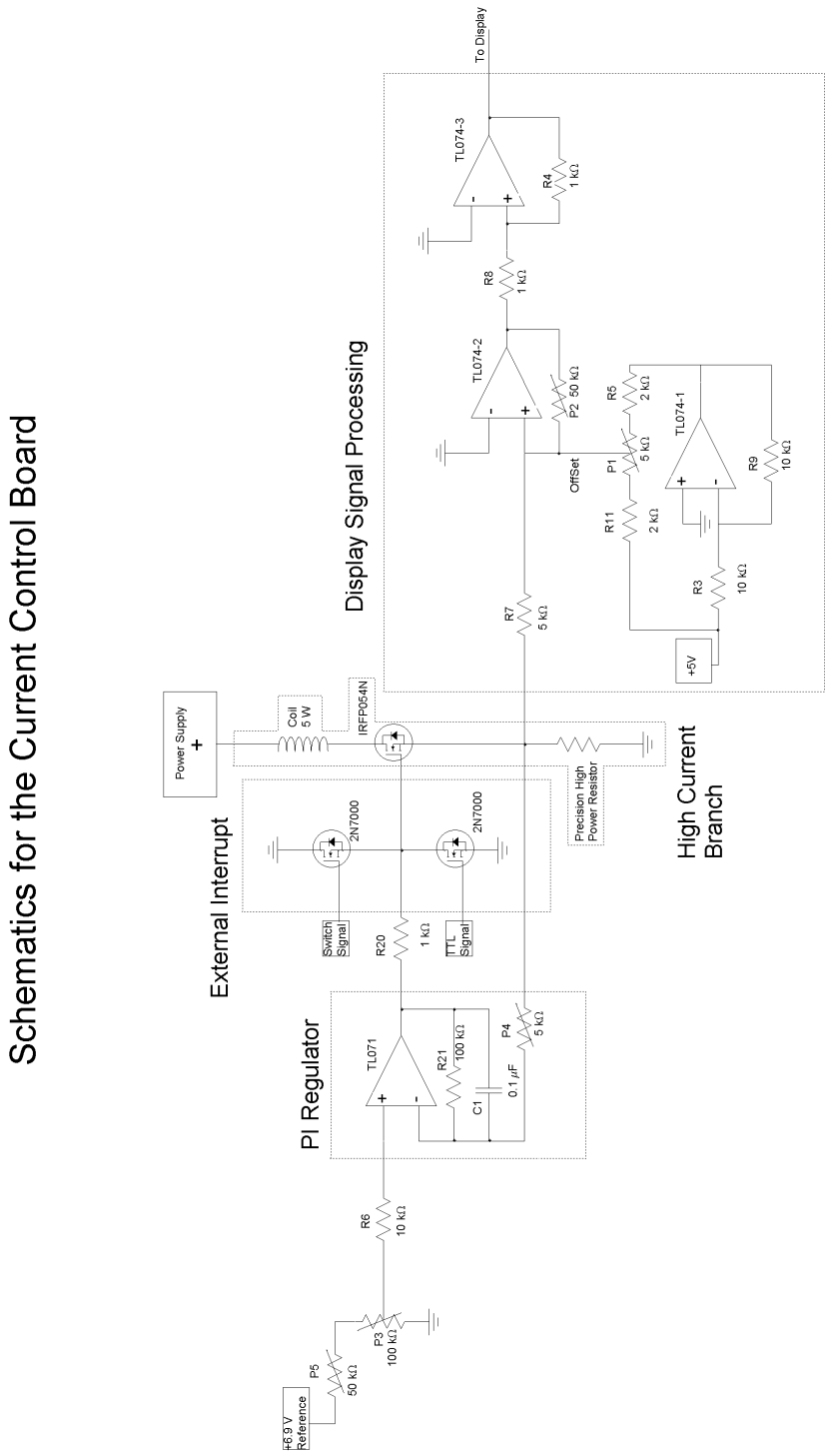

Figure 5.1: Schematics of the electronics that controls the current through the Zeeman slower coils.

- The IRFP054N Power MOSFET
- The Pickup Signal for Feedback and Display
- Signal Processing for the Display

It should be noted that the part of the board that controls the gate of the power MOSFET voltage is completely decoupled from the high currents that are run through the coils.

5.1.1 PI Regulator

The heart of the current regulation is a TL071 Low Noise Operational Amplifier (see Fig. 5.2) that works as a PI regulator. The P stand for *proportional*, since the operational amplifier uses the input difference to proportionally create an output. The I stands for *integration* and stands for the way capacitor C_1 is operated. This integrator ensures that the regulator reaches its set-point without offset. The operational amplifier's positive input is set to an adjustable reference voltage that is modified with a precision pentameter at the panel of the box. Its negative input is

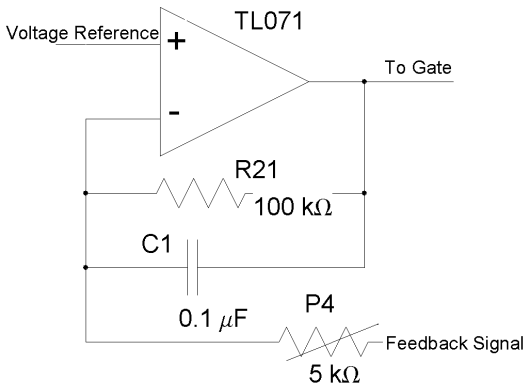

Figure 5.2: Magnification of the PI-Regulator out of Fig. 5.1

set to the feedback signal. The gain of the feedback loop is given by:

$$g = 1 + \frac{R_{21}}{P_4}. \tag{5.1}$$

By adjusting the trim pot P_4 the gain can be maximized when taking into account that the feedback loop starts to oscillate for too high a gain.

The integrating capacitor C_1 sets the frequency at which the amplification drops by 3 dB. This frequency is given as

$$f = \frac{1}{2\,\pi \cdot C_1 \cdot R_{21}}. \tag{5.2}$$

The frequency f should be chosen so that DC signals can still be amplified well whereas the amplification at 60 Hz should already be low enough not to amplify the line signal. Thus f was chosen to be about 15 Hz. For a value of $R_{21} = 100$ kΩ, we get a capacitance for C_1 of 0.1 μF.

The reference voltage is set by a precision potentiometer (100 kΩ) that is located at the front panel of the box. The maximum value of the reference voltage is 6.9 V (see section 5.3.1). This gives the maximum value that the feedback signal can have in order for the operational amplifier to still be able to regulate (see section 5.1.3). The voltage is limited by a trimpot (P_5), so that the maximum current that the coil should be run with is reached roughly at the clockwise end of the reference potentiometer. The output voltage of the operational amplifier is fed to the Power MOSFET that is described in the next section.

5.1.2 The Power MOSFET

The power MOSFET IRFP054N regulates the current flowing between its drain and source which corresponds to the voltage on the gate, hence controlling the current through the Zeeman slower coils (see Fig. 5.3). This MOSFET was chosen because it can handle high power dissipation (Maximum 170 W).

This is necessary since there is a large range of currents (some coils must be regulated

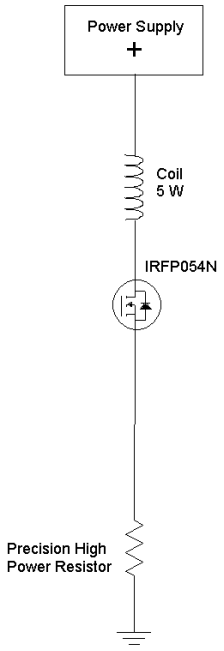

Figure 5.3: Schematics of the branch where the high currents through Zeeman slower coil, Power MOSFET, and precision resistor are flowing.

between 0 A and 5 A) and some voltages of the coils' voltage supplies (see section 5.3.2) are rather high; thus much voltage can drop between drain and source of the MOSFET leading to a high power dissipation at high currents. In the next paragraph a calculation for the power dissipation in the MOSFET is given.

Power Dissipation in a MOSFET

Fig. 5.3 shows a schematic of the high current branch. We assume that the FET keeps the current I constant. Since the voltage drop across the resistor R_{Coil} is given by $\Delta U_{\mathrm{Coil}} = R_{\mathrm{Coil}} \cdot I$, the voltage drop across the MOSFET must be:

$$\Delta U = U_{\mathrm{PS}} - R_{\mathrm{Coil}} \cdot I. \tag{5.3}$$

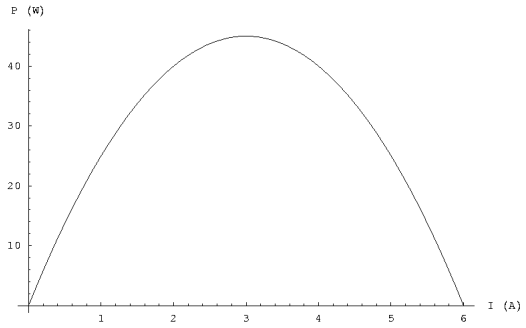

Figure 5.4: Plot of the power dissipation in a FET operated like shown in Fig. 5.3. The calculation assumes a resistance of the coil of 5 Ω, and a voltage of 30 V. The maximum power dissipation lies at 3 A and is $P = 45$ W.

Since the dissipated power in the FET is calculated by $P_{\mathrm{FET}} = \Delta U \cdot I$, the dissipated power is:

$$P_{\mathrm{FET}} = U_{\mathrm{PS}} \cdot I - R_{\mathrm{Coil}} \cdot I^2. \tag{5.4}$$

A plot of this function is shown in Fig. 5.4, assuming a resistance of the coil of $R_{\mathrm{Coil}} = 5\Omega$, and a power supply voltage of $U_{\mathrm{PS}} = 30\ V$. The maximum power dissipation occurs at $I(P = P_{\mathrm{max}}) = \frac{U_{PS}}{2 \cdot R}$ and the maximal power dissipated is $P_{\mathrm{max}} = \frac{U_{PS}^2}{4 \cdot R}$. Using the numbers given above, we get a maximum power dissipation of $P_{\mathrm{max}} = 45\ W$, at current $I(P_{\mathrm{max}}) = 3\ A$. This shows that the maximum power dissipation lies within the range over which the FET has to regulate.
Though the IRFP054N is designed to deal with high power, the FET has to be mounted to a heat sink to conduct the heat away from it. Air is blown over the heat sink to provide effective cooling.

5.1.3 The Pickup Signal

For the feedback and for the display that shows the current flowing through the MOSFET and coil, a voltage has to be picked up that does not change much with

temperature. For this purpose we use a high power precision resistor. The value of this resistor changes depending on what current is flowing through it. The voltage drop across the resistor must be large enough to clearly exceed the noise level. Otherwise the gate voltage, and hence the current through the coil, would carry a strong noise signal. On the other hand, the pickup voltage across the resistor for the highest current used in the particular coil must be smaller than the maximum possible reference voltage provided (in this case 6.9 V). This leads to the values of resistors given in Table 5.1. To temperature stabilize the resistor, it is mounted onto a heatsink.

# coils	I/A	R/Ω	Pickup signal/V
1	4.64	0.1	0.464
2	3.44	1	3.44
3	3.12	2	6.24
4	2.68	2	5.36
5	2.28	2	4.56
6	1.83	2	3.66
7	1.34	4	5.36
8	0.79	6	4.74
9	0.18	10	1.80
10	-0.63	6	3.78
11	-1.22	4	4.88
12	-4.87	0.3	1.46
13	+1 ...+2	2	2...4

Table 5.1: Values for the resistors used depending on the current flow through the respective coil. The pickup voltages are given together with the resistances.

5.1.4 Display

To see which current is flowing through one particular coil, the voltage drop across the resistor is processed and works as the input signal of a Keithley Acculex DP-650 Digital Panel Meter (see Fig. 5.5). The display expects an input between 0 and 200

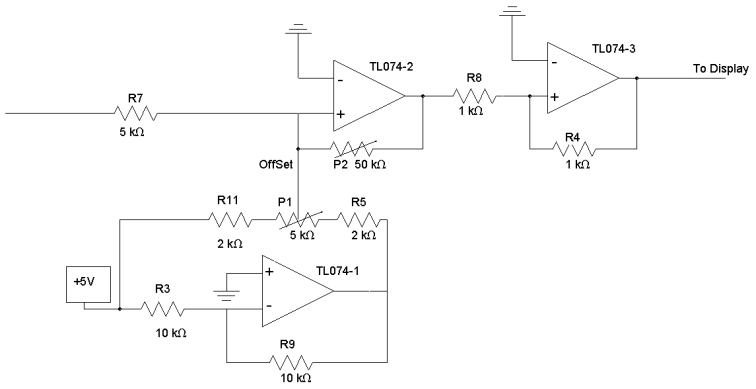

Figure 5.5: Schematics of the electronics part that processes the signal for the display.

mV, and the pickup signal depends on the resistor used. Setting of the parameters (a) offset (ΔI) and (b) slope ($\frac{\partial I}{\partial U}$) is needed to match the displayed current I_D to the real flowing current. The displayed value changes with the pickup signal as:

$$I_D = \Delta I + U_{Pickup} \cdot \frac{\partial I}{\partial U}.$$

An offset regulation was introduced (trim-potentiometer P_1) to adjust the zero point of the display. The signal is fed through an operational amplifier (TL074 Quad operational amplifier) with adjustable gain (trimpot P_2) to change the slope ($\frac{\partial I}{\partial U}$). Because the signal so far has the wrong sign, its sign is flipped by a unity gain inverter (TL074 Quad operational amplifier). The resulting signal can be used as input signal for the display.

5.1.5 External Interrupt of the Current

By pulling the gate of the power MOSFET to ground, a current flow from drain to source can be stopped. This method can be used as a switch to turn off the current and is used in two cases. In the first case, a FET (2N7000) gate is opened by an

external panel switched voltage, connecting the gate of the power MOSFET with ground (Fig. 5.1). In the second case, the TTL signal of the temperature interlock board (see section 5.2) can open a gate of a 2N7000 FET to pull the gate of the power MOSFET to ground (see Fig. 5.1).

5.1.6 Adjusting a Current Control Board

In this section we describe how a new board should be adjusted so that the feedback works with maximal gain and without oscillations. The circuit has to be connected as shown in Fig. 5.1. It should be monitored by an external amp-meter and the pickup signal should be fed to an oscilloscope. The procedure is as follows:

- With connected power supply and coil, turn the precision potentiometer (Schematics P_3) to its clockwise (cw) end. The current in the coil should increase after about one turn.
- With trimpot P_5, adjust the current to the highest needed value.
- Tune the oscilloscope to a range (AC coupled) where the noise of the pickup signal is hardly visible against the ground-line.
- Increase the gain with trimpot P_4 (the current should increase) until large oscillations appear on the oscilloscope. Tune the gain back until the oscillations completely disappear.
- Readjust trimpot P_5 for the highest needed current.
- Bring the precision potentiometer P_3 to its counterclockwise (ccw) end; there must not be any oscillations over the whole range.

The adjustment for the display works as follows:

- Switch the display to the right board with the rotary switch next to the display on the front panel.

- With the precision potentiometer at the cw end (the current in the coil should be 0 A), turn trimpot P_1 to bring the display to "0.00".
- Increase the current in the coil all the way to the maximum, and adjust trimpot P_2 until the value shown by the display and by the amp-meter match.
- Bring P_3 back to the ccw end, and check whether both the amp-meter and the values shown by the display match over the whole range.
- If necessary, adjust P_1 again, and repeat this until the display shows the right current in all situations.

5.2 Temperature Interlock

Since it is possible that by a malfunction of the controlling unit too much current can flow through the coils leading to a very high temperature, a circuit (for schematics see Fig. 5.6) was designed to monitor the temperature. It reads out the signal of a thermocouple that was wound into the inner cylinder of two coils. If this signal exceeds an adjustable threshold, it triggers a flip-flop that sends a TTL signal which pulls the gates of the power MOSFETS to ground (see section 5.1.5).

5.2.1 Operation Breakdown of the Temperature Interlock

The incoming thermocouple signal is amplified by an inverter (TL071 operational amplifier) with adjustable gain (trimpot P_2). It is then compared with a settable threshold signal (adjusted by trimpot P_3) in a TL071 operational amplifier. The output is inverted and amplified in a TL071, since the flip-flop 7474 can only take inputs up to 6 V. The flip-flop setup is not standard and shown in Fig. 5.7. The output of the last operational amplifier is not put into the `Data` pin as usual, but into the `Clear` input, whereas the `Data` and `Clock` inputs are grounded. In normal operation (input signal is high when temperature is below threshold, and `Preset`

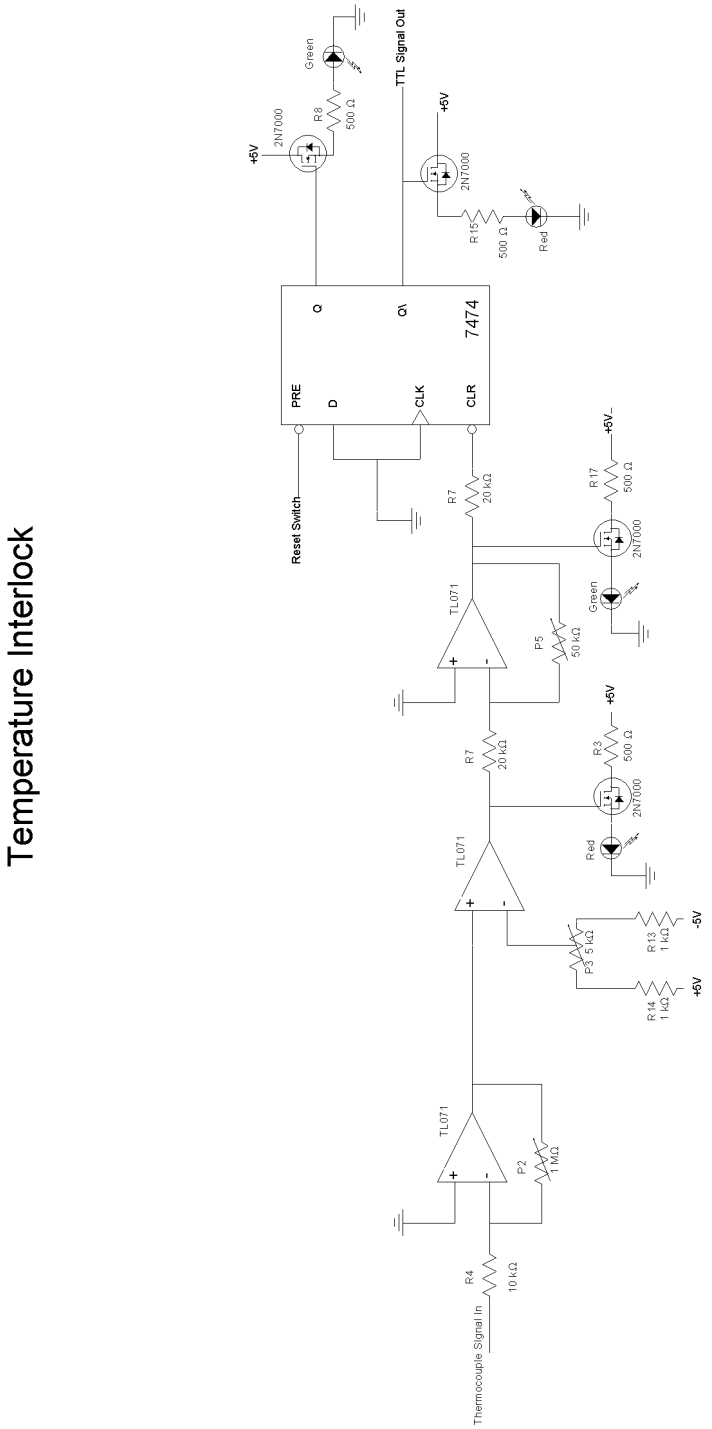

Figure 5.6: Schematics of the circuit board used as Temperature Interlock; the signal of a thermocouple is read out, compared with a reference, and in case of exceeding a threshold, a TTL signal is put out that can be used to interrupt the current through the coils (see Section 5.1.5).

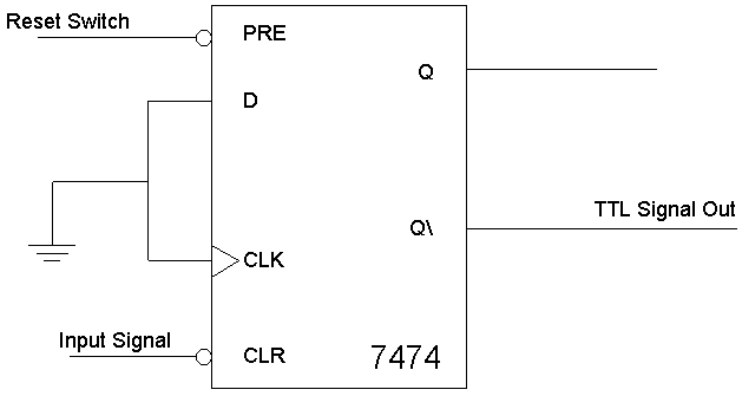

Figure 5.7: Schematics of the Flip-flop Connection for the used 7474 chip. The data and clock input are grounded whereas the signal is fed to the clear pin.

is high) the output Q is high. When the `Clear` input switches to low, the output switches as well (output $\overline{Q}$ is high). It can then be reset by momentarily setting the `Preset` to low (ground). The signal from output $\overline{Q}$ can be fed to the gate of a 2N7000 FET on a board to control the gate of the power MOSFET (see section 5.1.5).

5.2.2 Adjusting a Temperature Interlock Board

To adjust the temperature interlock board, a Type K thermocouple and a heater for it are needed; moreover, the temperature of the heater should be measured by an independent device. The adjustment should be done based on the following steps:

- Adjust trimpot P_2 so that the thermocouple signal has a value of about 0.5 V at 300° C.
- Adjust trimpot P_3 so that the negative input of the second TL071 has the same value as the output of the first TL071 at the heater temperature where

the circuit shall switch.

- Adjust trimpot P_5 so that the output of the third TL071 lies between -6V and +6V (since the flip-flop 7474 cannot handle more than ±7V input).

5.3 Assembly of the Electronics

In order to control the operation of thirteen coils, three boxes were assembled, two of them containing the electronics for four coils and one for five coils. In addition to the current control boards, each box contains one temperature interlock board, one board to create the reference voltages (see section 5.3.1), one board to distribute those voltages, and one board to control the signals for the display. The basic arrangement of the boards are is shown in Fig. 5.8.

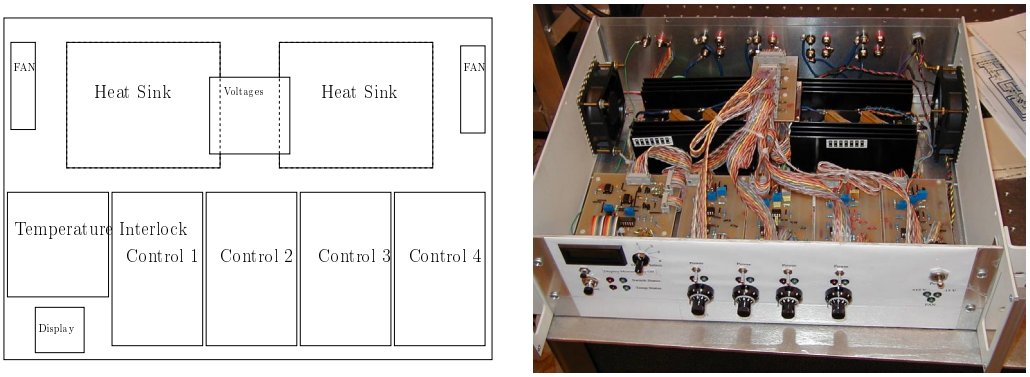

Figure 5.8: Schematics of the inside of a control box (left side) and a picture of the inside of the box (right side).

5.3.1 Reference and Supply Voltages

In order for the operational amplifiers to work, voltage supplies of ± 15 V are needed. Those voltages are externally supplied (see section 5.3.2). Reference voltages for the adjustment of the currents through the coils are necessary, as well as for the setting

of the threshold of the temperature interlock or the offset of the display. The 7474 flip-flop needs a supply voltage of +5V, the LEDs on the front panel are driven by +5V, and the gates of the 2N7000 FETs are completely opened at +5V.

In order to minimize changes in the critical reference voltage, a LM399 voltage reference was used. The LM399 is a temperature stabilized zener diode with a breakdown voltage of 6.9 V. The noise level lies well below 0.1%[†]. A +5V voltage supply is created by a 7805 chip; this voltage drives all the parts that need current, such as LEDs or the display. A schematic of the board that creates all the voltages is given in Fig. 5.9. All the signals in the boxes are conducted by twisted pair cables

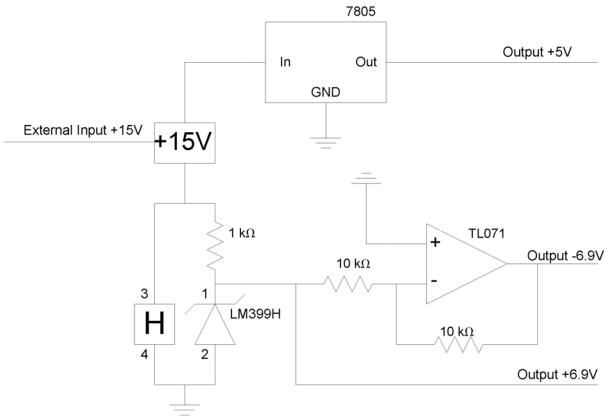

Figure 5.9: Schematics of the circuit board that creates the reference voltages (± 6.9 V) and the supply voltage (+ 5V) for LEDs.

or twisted pair flat cable. The voltages are distributed to the boards by twisted pair flat wire, the voltages to panels or the display run through twisted pair wire.

[†]The noise levels are calculated relative to the DC signal of the oscilloscope

5.3.2 Voltage Supplies for the Coils

Depending on how much current a particular coil needs, a power supply with corresponding voltage and current values was chosen. In the following, a quick description of the power supplies used is given.

Supply Voltages

The ±15 V voltages were created by two Power Ten Voltage Supplies # 91004-15V/5A. A Lambda power supply LXS-D-28-R that is adjusted to 30V drives the cooling fans for cooling the coils and the power supplies in the rack. The fans are NBM 4710NL-04W-B50D00, 12 V DC fans. A pair of fans is connected in series and driven by 30V. The Lambda drives a total of ten pairs of fans with a total current of 3 A output of the Lambda power supply.

Coil power supplies

The type of power supply used varies as well as the used voltage in this supply. In Table 5.2 the power supply for each coil and the calculated current are given.

5.4 Problems of the Electronics

Since the electronical regulation was not professionally built, but part of a learning process, there are still some minor problems left that one should note when operating the Zeeman slower.

Ground Level Shifting

One problem deals with the fact that the used wires in the boxes have finite resistance. The level of ground is propagated from the Power Ten Voltage Supplies to each box. Within the box, the ground is distributed from the reference voltage

#	I/A	U/V	Type
1	4.64	24	LXS-D-28-R
2	3.44	24	LXS-D-28-R
3	3.12	24	LXS-D-28-R
4	2.68	24	LXS-D-28-R
5	2.28	24	LXS-D-28-R
6	1.83	24	LXS-D-28-R
7	1.34	18	LM C24
8	0.79	15	LND-X-152
9	0.18	8	LCS-A-5-0V
10	-0.63	15	LND-X-152
11	-1.22	15	LM C12
12	-4.87	24	LXS-D-28-R
13	1...2	24	LXS-D-28-R
FAN	—	30	LXS-D-28-R

Table 5.2: Table of the used power supplies and the respective voltages for the coils of the Zeeman slower.

board (see section 5.3.1) to the power supplies for the coil, to the circuit boards within the box, and to the front panel. Since high current is flowing through some of the coils, the ground level shifts if such a coil is suddenly switched on. The wires used in the box for ground have a finite resistance, thus the shift is not uniform, but a voltage drop can be measured. This difference in the ground level can be of the order of a few tens of millivolts. This leads to a shift in the pickup signals of the feedback loops and a shift in the currents of the other coils, no matter whether they are controlled by the same box or by another one. The change in the current can be up to 200 mA. Unfortunately, the shift in the current is not displayed on the box LCD, since the ground level of the display shifts together with the changing current.

It is highly recommended to preadjust all the currents as given in Tab. 3.1, and adjust them again with all the other coils switched on. Also, I suggest the usage of

an external amp-meter to monitor the current in the coil.

Flat Ribbon Cable Connectors

Most of the signals to and from the current control boards are transported by flat ribbon cable. The big advantage is that connections can be quickly removed and thus boards can be changed easily and fast.
However, in some cases the problem occurred that after several connecting - unconnecting cycles, a signal wire was shorted to a shielding ground wire. In case of strange behavior of one circuit or box, it is recommended to remove all ribbon cable connectors, reconnect them successively, and replace a cable, if the problem appears when it was connected.

Flip-flop

The flip-flop 7474 used in the temperature interlock circuit is sensitive toward changes of voltages. When the Zeeman slower is started, usually the flip-flop output $\overline{\mathrm{Q}}$ is high, interrupting the current through the coils. However, it might happen that switching a box on or off affects the flip-flops of the others. In usual operation all boxes are switched on, thus this problem does not occur.

Chapter 6

The Magnetic Field of the Slower

After assembling the coils and the electronics, the magnetic field of the Zeeman slower was characterized. The coils were driven by the currents calculated in the simulation. The DC and AC components of the field were measured up to 400 Hz*, and a Fourier analysis was performed. Finally the temperature stability of the magnetic field and the field components in the directions perpendicular to the z-axis were measured.

The data of the measurements are compared with calculations, and the field gradient is calculated for the measured field and compared to the limit given by the adiabatic following condition.

6.1 Measuring the Magnetic Field

The magnetic field in z-direction is measured with the coils driven by the currents given in table 3.1 at points separated by 0.5 inches (1.27 cm). The graph of the

*The Gauss-meter used is a F. W. Bell Series 9550 Gauss/Tesla-meter and limited to a range between DC and 400 Hz

measured points (red points) together with the calculated field (blue curve) and the ideal field (black curve) is shown in Fig. 6.1. As before, the data points are

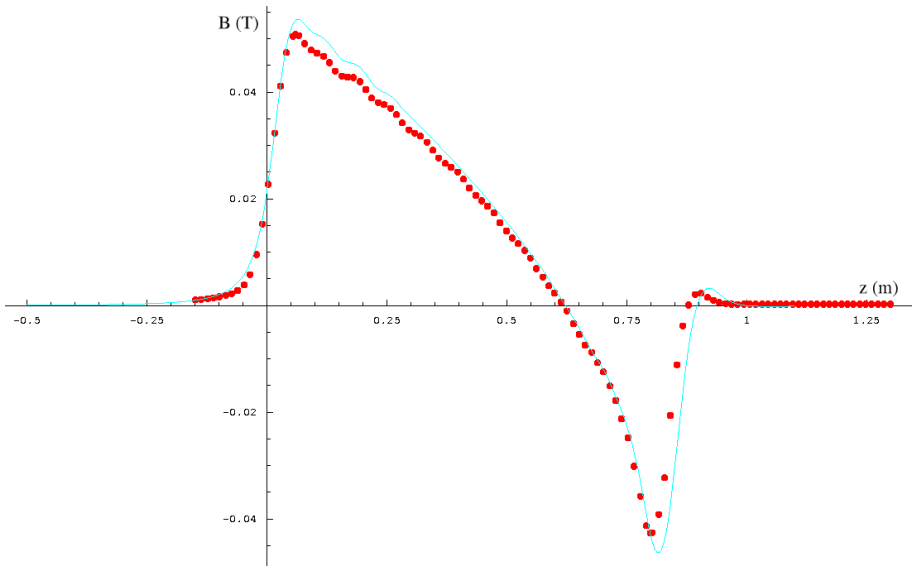

Figure 6.1: Graph of the measured magnetic field (red dots) together with the simulated field (blue line) for the used coil geometry. The shape of the field matches well, whereas the deviation in absolute value of the magnetic field strength at the ends of the slower are due to the imperfect winding of the coil. Since the simulation used a small gap between slower and extraction coil but the built slower does not, the two bumps in the field shape at the end of the slower do not match.

interpolated and the field gradient for this interpolating function is calculated. The graph of this is shown in Fig. 6.2 as orange line together with the simulated gradient (blue line) and the adiabatic following limit (red line). As was mentioned in section 3.1.1 the field created by the multiple coil Zeeman slower deviates from the ideal shape at some points due to the rather small number of steps compared with a tapered solenoid. However, since the slower was designed to operate in a regime far away from the limit of adiabatic following, there is no danger of loosing atoms from the slowing, as can be seen in Fig. 6.2.

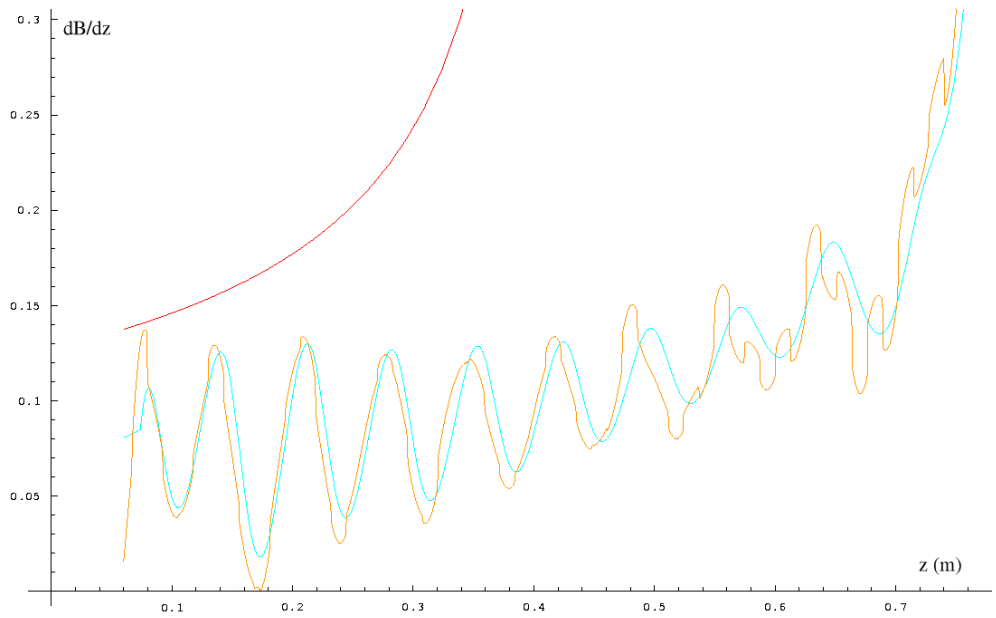

Figure 6.2: Magnetic field gradient of the measured and interpolated magnetic field strength (orange line), the simulated gradient for the same geometry (blue line) and the limit given by the adiabatic following condition (red line). The measured field never violates the adiabatic field condition.

6.2 Noise of the Field and Perpendicular Field Components

The noise of the field was measured at eight points and gave a mean noise level of 2.1%[†]. The noise measured at one representative point is shown in Fig. 6.3 together with the Fourier transform of this function. Since the highest frequency

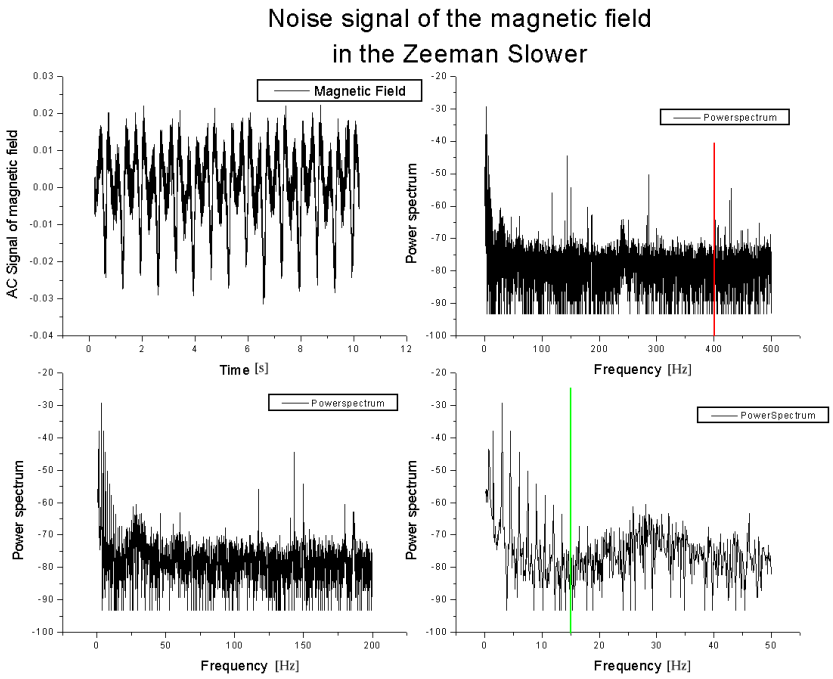

Figure 6.3: Measured Noise of the Zeeman slower. The first graph gives a ten second record of the noise within the slower. The second graph is the Fourier transform of this noise. Since the Gauss-meter can only detect noise up to 400 Hz, only the region with $f \leq 400$ Hz is relevant (left of the red line). The next two graphs magnify the low frequency domain. The low frequency components are likely intrinsic oscillations of the electronical regulations and do not affect the slowing at all; the green line marks the cut-off frequency of the PI regulator.

[†]Relative to the DC signal

that the Gauss-meter can resolve is 400 Hz, corresponding to a period of 2.5 ms. The traveling time of an atom through the Zeeman slower varies between 2 ms for atoms traveling with 1000 $\frac{\mathrm{m}}{\mathrm{s}}$ and 100 ms for atoms traveling with 10 $\frac{\mathrm{m}}{\mathrm{s}}$, thus this noise might have an effect on the slowing of the atoms. However, the measured noise level of 2.1% corresponds to a noise of approximately 100 mA; this case was covered in a simulation and showed no violation of the adiabatic following condition (see section 3.3.2).

The even higher frequency noise that could affect the slowing is very likely damped by the inductance of the coil and does not exceed the noise level of 2%.

The low frequency noise that is shown in Fig. 6.3 does not affect the slowing, because the traveling time of the atoms is short compared to the period of those oscillations. This low frequency noise is very likely to be intrinsic to the electronic regulation, since the cut-off frequency of the PI regulator was chosen to be $f = 15$ Hz (see section 5.1.1).

The components of the magnetic field that are perpendicular to the z-axis were measured at eight points along the slower; the values for the transverse components range like:

$$\begin{aligned} -10\ G \leq \mathcal{B}_x \leq +6\ G \\ -2\ G \leq \mathcal{B}_y \leq +1\ G \end{aligned} \tag{6.1}$$

Chapter 7

The Zeeman Slower's Environment

The Zeeman slower is only one part of our cold atoms source. This source produces a high (10^{10} $\frac{\text{atoms}}{\text{s}}$) flux of cold sodium atoms in ultra high vacuum (10^{-10} Torr). In this chapter we will briefly describe the other components of the experimental setup that work together with the Zeeman slower.

The slower is located between the thermal atom source on the one side, consisting of an oven, collimation, differential pumping pipe, and optical molasses region, and the science chamber on the other side.

7.1 Thermal Atom Source

7.1.1 The Candlestick Oven

The oven design is based upon the so-called *Candle Stick* design [8, 11]. The main advantage of this design compared with usual vapor cell ovens is the recycling of not emitted sodium. Thus the loading frequency for such a candlestick oven is very low.

Differential Pumping

The pressure in the oven is expected to be of order 10^{-8} Torr, pumped by a turbo pump. However, in the main chamber a pressure of 10^{-11} Torr is needed; a 270 $\frac{\text{l}}{\text{s}}$ ion pump is employed on this side of the Zeeman slower.
To assist in maintaining a pressure differential between the oven side and the main chamber side of the Zeeman slower, a differential pumping tube (a piece of tubing with decreasing diameter) is placed after the oven in a bellows to lower the gas conductance between the oven and Zeeman slower.

7.1.2 Collimation of the Atom Beam

In our experiment, the atoms have to fly over a distance of about 180 cm between their release from the oven to their capture in the science chamber. If the atom beam was emitted uncollimated from the oven into the Zeeman slower, many atoms would bounce against the walls of the vacuum pipe. Those atoms do not contribute to the output flux of the Zeeman slower, but they can increase the background pressure in the science chamber and disturb the experiments with the trapped atoms.
To avoid this kind of problem, ideally all atoms entering the Zeeman slower shall be slowed down. For this purpose, two devices were employed in the experimental setup.

Collimation Tube

Immediately after the atoms leave the oven, they have a divergence that is determined by the diameter of the oven nozzle. In our case, the atoms are emitted in a solid angle of $\frac{1}{25}$ sr, as we deduce from an experiment with similar geometry [11]. Most of the atoms in this geometry will not clear the Zeeman slower. Because of that, a collimation pipe is inserted into the way of the atoms, lowering the solid angle to $3 \cdot 10^{-3}$ sr. Still not all atoms clear the Zeeman slower tube, and the final

solid angle into that the slow atoms are emitted at the end of the slower, is $5 \cdot 10^{-6}$ sr.

From these values, we can estimate the mean velocity of the atoms perpendicular to the z-axis. We assume a most probable velocity in the atomic beam of $v_{\mathrm{mp}} = \sqrt{\frac{9\,\pi}{8}} \cdot \sqrt{\frac{k_{\mathrm{B}}\,T}{m}} = 800\,\frac{\mathrm{m}}{\mathrm{s}}$. With a half angle of $\frac{\delta}{2} = 1.7^\circ$ (corresponding to a solid angle of $3 \cdot 10^{-3}$ sr), we get a highest transverse velocity of $v_\perp^{\mathrm{max}} = 800\,\frac{\mathrm{m}}{\mathrm{s}} \cdot \sin(1.7^\circ) = 22\,\frac{\mathrm{m}}{\mathrm{s}}$. It should be noted that this result is one order of magnitude larger than the heating in transverse direction due to the random walk of the atoms in the Zeeman slower $\Delta v_\perp = 2.9\,\frac{\mathrm{m}}{\mathrm{s}}$ (see section 1.4.3).

Optical Molasses

As we just estimated, the transverse velocity of the atoms leaving the collimation tube can be up to $22\,\frac{\mathrm{m}}{\mathrm{s}}$ An atom with a higher transverse velocity is more likely to reach the Zeeman slower wall. After a collision with the wall an atom is not likely to contribute to the final flux. To minimize this loss process, the atoms are cooled in the transverse directions by two-dimensional optical molasses before entering the Zeeman slower. The resulting decrease in the divergence of the atomic beam should increase the output flux of the Zeeman slower by a factor of two.

The working principle of optical molasses has been described in section 1.2. It should be noted again that this configuration of two-dimensional optical molasses cools the atoms but does not compress them.

7.1.3 Gate Valve

Between the two-dimensional optical molasses and the Zeeman slower, there is a all-metal gate valve that is normally open during operation. If it is completely closed, vacuum can be broken on the oven side without affecting the main chamber. A major concern is a failure of the pumps on the oven side. This valve can, even if

it is not completely closed, provide protection against flooding the science chamber with sodium.

7.2 The Science Chamber

After the Zeeman slower, the atoms enter the science chamber which has a target pressure of 10^{-10} Torr. This chamber is pumped by a 270 $\frac{\text{l}}{\text{s}}$ ion pump. In the science chamber a MOT will capture the atoms exiting the Zeeman slower. The high flux of slow atoms exiting the Zeeman slower will provide a large MOT (10^{10} atoms for a 1 s loading period). By application of other standard cooling techniques such as evaporative cooling, formation of a Bose-Einstein Condensate should be possible.

Appendix A

Universal and Sodium Specific Constants[12]

Physical Constants		
Speed of Light	c	$2.997 \cdot 10^{8}$m/s
Planck's Constant	$\hbar$	$1.0546 \cdot 10^{-34}$ J·s
Bohr Magneton	μ_{B}	$9.274 \cdot 10^{-24}$ J/T
Boltzmann's Constant	k_{B}	$1.381 \cdot 10^{-23}$ J/K

Sodium		
Atomic Mass	m	$3.818 \cdot 10^{-26}$ kg
Nuclear Spin	I	3/2

Sodium D2 Transition		
Wavelength (Air)	λ	589.00 nm
Lifetime	τ	16.25 ns
Decay Rate	γ	$61.542 \cdot 10^{6}$ s^{-1}
Recoil Velocity	$\delta v_{\mathrm{recoil}}$	2.946 cm/s

Table A.1: Table of fundamental constants and sodium data frequently used in the text.

Appendix B

Eagle Schematics of the Circuit Boards

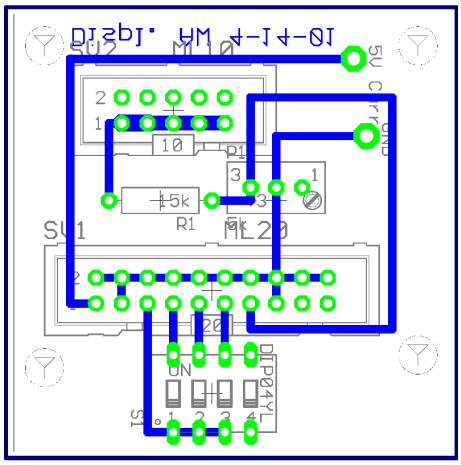

Figure B.1: Board for the display

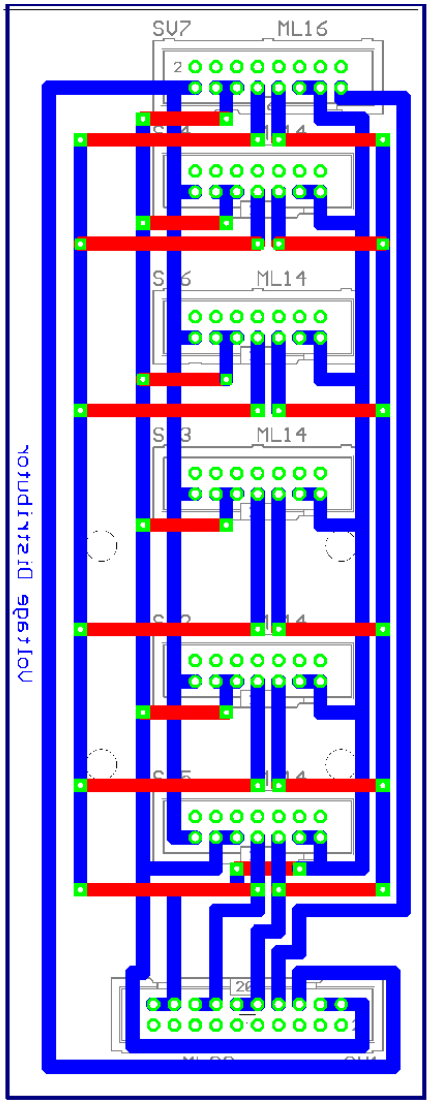

Figure B.2: Board for the distribution of the voltages.

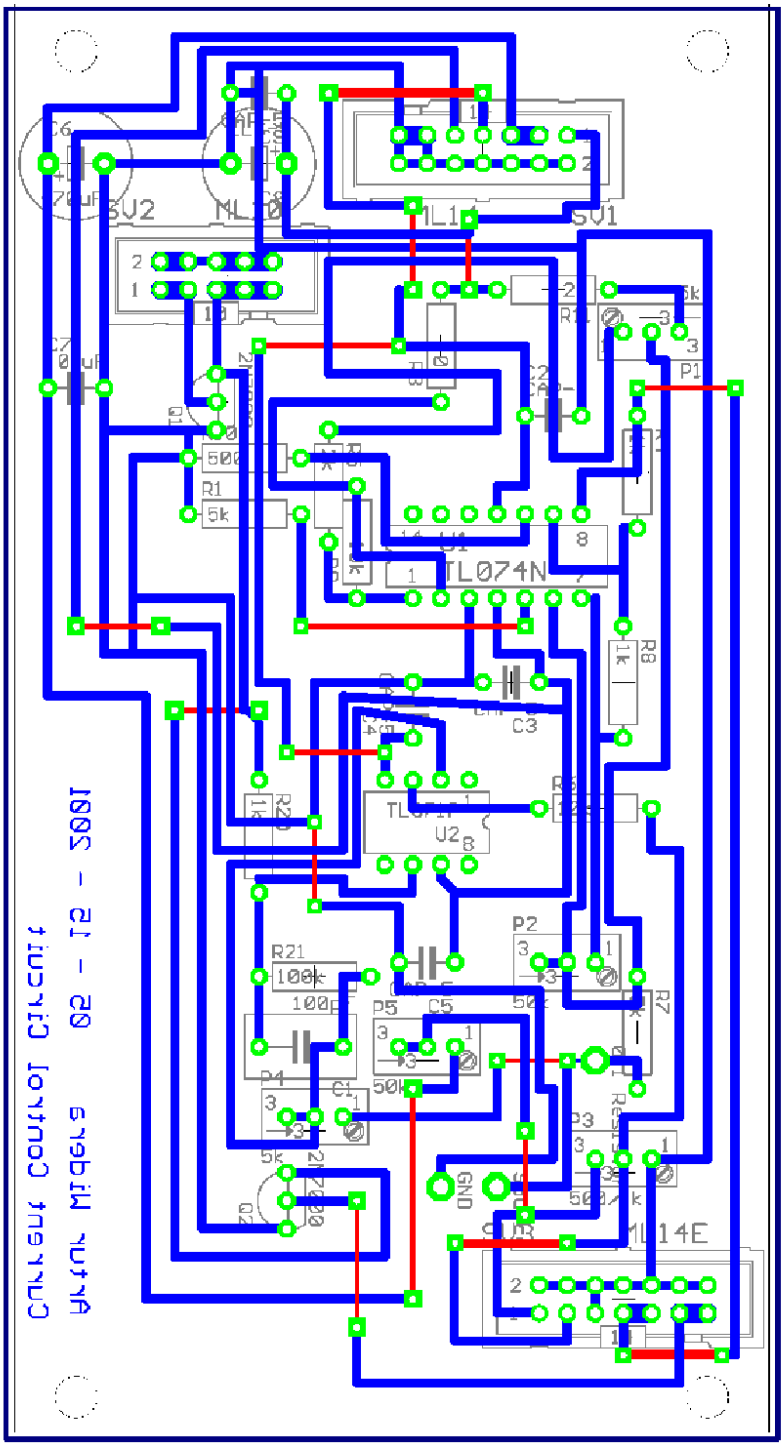

Figure B.3: Board for the current control of the coils.

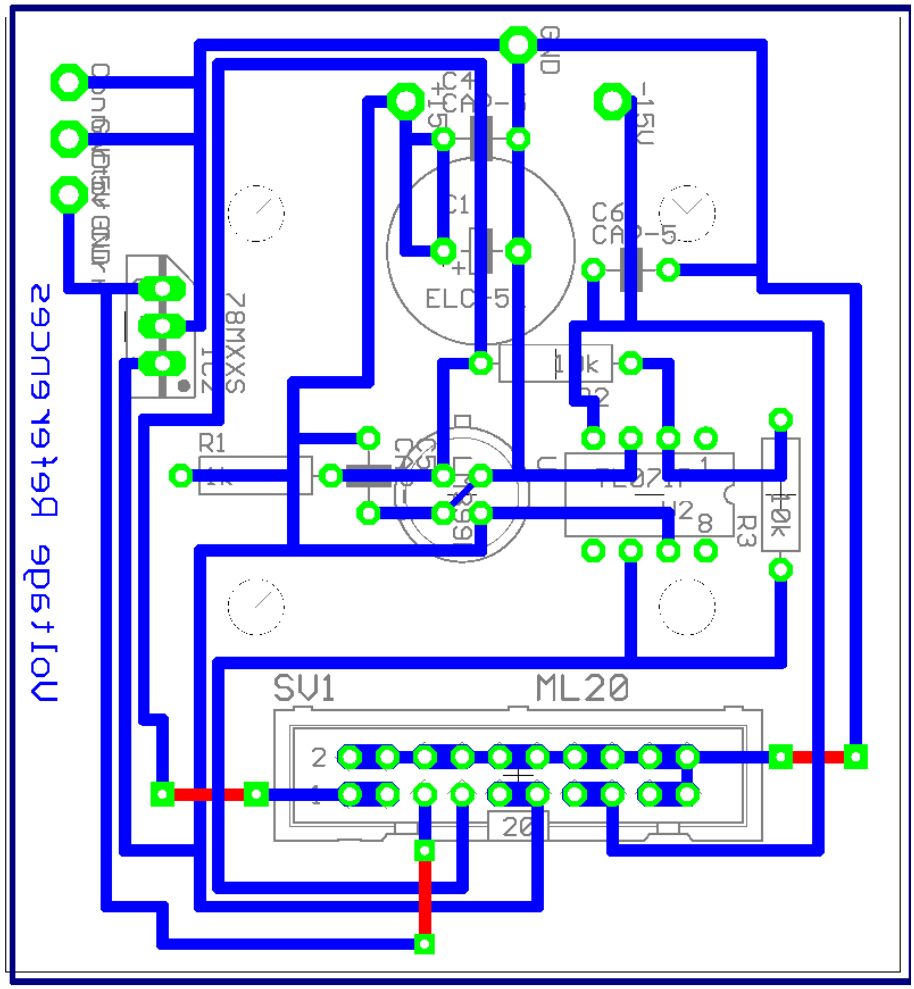

Figure B.4: Board that creates the reference voltages.

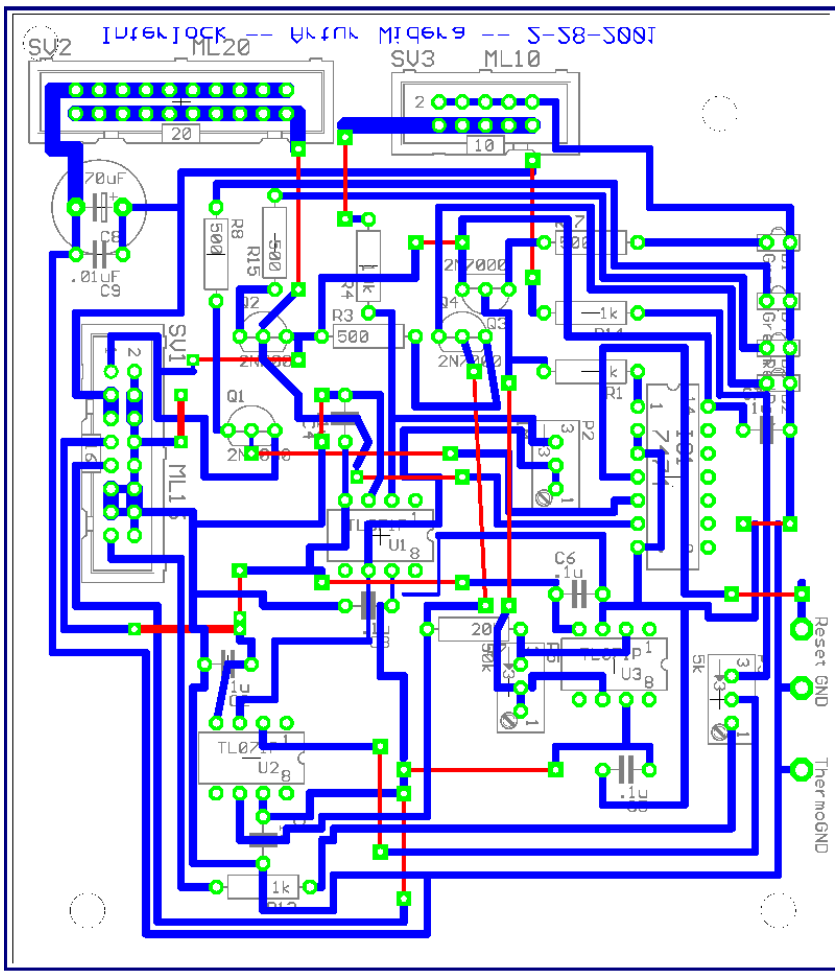

Figure B.5: Board for the monitoring of the temperature and the interrupt of the current.

Bibliography

[1] W. D. Phillips, and H. Metcalf;
Laser Deceleration of an Atomic Beam; Phys. Rev. Letters, Vol. 48, No. 9, March 1982

[2] S. Chu, L. Hollberg, J. E. Bjorkholm, A. Cable, and A. Ashkin;
Three-Dimensional Viscous Confinement and Cooling of Atoms by Resonance Radiation Pressure; Phys. Rev. Letters, Vol. 55, No. 1, July 1985

[3] H. Metcalf, P. van der Straten;
Laser Cooling and Trapping; Springer-Verlag 1999

[4] B. H. Bransden, C. J. Joachain;
Physics of atoms and molecules; Longman Scientific & Technical; 1992

[5] F. Reif;
Fundamentals of Statistical and Thermal Physics; McGraw 1965

[6] A. Aspect, E. Arimondo, R. Kaiser, N. Vansteenkiste, and C. Cohen-Tannoudji;
Laser Cooling below the One-Photon Recoil Energy by Velocity-Selective Coherent Population Trapping; Phys. Rev. Lett., Vol. 61, No. 7, pp. 826, August 1988

[7] V.S. Bagnato, G.P. Lafayatis, A. Martin, K. Helmerson, J. Landry, and D. E. Pritchard;

Laser deceleration and velocity bunching of a neutral sodium beam; J. Opt. Soc. Am. B, Vol. 6, No.11, November 1989

[8] B. D. Bush;
Bose-Einstein Condensation and Atomic Interactions in a Sodium Gas; Ph. D. Thesis; January 2000

[9] D. S. Durfee; *Dynamic Properties of Dilute Bose-Einstein Condensates*; Ph. D. Thesis; August 1999

[10] U. Tietze, Ch. Schenk;
Halbleiter-Schaltungstechnik; Springer-Verlag 2000
English version: *Electronic Circuits Design and Applications*; Springer-Verlag 1991

[11] L. V. Hau, J. A. Golovchenko, M. M. Burns;
A New Atomic Beam Source: The "Candlestick"; Rev. Sc. Instr., Vol. 65, No. 12, December 1994, pp. 3746-50

[12] D. A. Steck;
Sodium D Line Data;
http://www.ph.utexas.edu/∼quantopt/resources/sodiumnumbers.pdf

.

Vita

Artur Widera was born on June 30, 1977 in Fulda, Germany as the son of Dr. Hans Widera and Hildegard Widera. He received his Abitur from the Freiherr-vom-Stein-Schule in Fulda 1996. The next thirteen months he spent in mandatory civil service. He started studying physics at the Bayerische Julius Maximilians Universität Würzburg in November of 1997. After receiving his Vordiplom in August 1999 and studying physics for one additional year in Würzburg, he entered the graduate school at the University of Texas at Austin in August 2000. Since January 2000 he has been a scholar of the Studienstiftung des deutschen Volkes (German National Merit Foundation).

Permanent Address: Stresemannstraße 13; 36039 Fulda; Germany

This thesis was typeset with LaTeX 2_ε* by the author.

*LaTeX 2_ε is an extension of LaTeX. LaTeX is a collection of macros for TeX. TeX is a trademark of the American Mathematical Society. The macros used in formatting this thesis were written by Dinesh Das, Department of Computer Sciences, The University of Texas at Austin.